2010-12-15

Modeling and Testing of DNA Motion for Nanoinjection

Regis Agenor David
Brigham Young University - Provo

Modeling and Testing of DNA Motion for Nanoinjection

Regis A. David

A dissertation submitted to the faculty of
Brigham Young University
in partial fulfillment of the requirements for the degree of

Doctor of Philosophy

Brian D. Jensen, Chair
Larry L. Howell
Sandra H. Burnett
Kenneth W. Chase
Aaron R. Hawkins

Department of Mechanical Engineering

Brigham Young University

April 2011

ABSTRACT

Modeling and Testing of DNA Motion for Nanoinjection

Regis A. David

Department of Mechanical Engineering

Doctor of Philosophy

A new technique, called nanoinjection, is being developed to insert foreign DNA into a living cell. Such DNA transfection is commonly used to create transgenic organisms vital to the study of genetics, immunology, and many other biological sciences. In nanoinjection, DNA, which has a net negative charge, is electrically attracted to a micromachined lance. The lance then pierces the cell membranes, and the voltage on the lance is reversed, repelling the DNA into the cell. It is shown that DNA motion is strongly correlated to ion transport through a process called electrophoresis. Gel electrophoresis is used to move DNA using an electric field through a gel matrix (electrolytic solution). Understanding and using electrophoretic principals, a mathematical model was created to predict the motion (trajectory) of DNA particles as they are attracted to and repulsed from the nanoinjector lance.

This work describes the protocol and presents the results for DNA motion experiments using fabricated gel electrophoresis devices. Electrophoretic systems commonly use metal electrodes in their construction. This work explores and reports the differences in electrophoretic motion of DNA (decomposition voltage, electrical field, etc.) when one electrode is constructed from a semiconductor, silicon rather than metal. Experimental results are used to update and validate the mathematical model to reflect the differences in material selection.

Accurately predicting DNA motion is crucial for nanoinjection. The mathematical model allows investigation of the attraction/repulsion process by varying specific parameters. Result show that the ground electrode placement, lance orientation and lance penetration significantly affect attraction or repulsion efficiency while the gap, lance direction, lance tip width, lance tip half angle and lance tip height do not. It is also shown that the electric field around the lance is sufficient to cause localized electroporation of cell membranes, which may significantly improve the efficiency of transport.

Keywords: BYU, MEMS, nanoinjector, DNA motion modeling, electrophoresis

ACKNOWLEDGMENTS

This work has been supported in part by the Microbiology & Molecular Biology department, the Ira Fulton College of Engineering and Technology at Brigham Young University, a BYU graduate research fellowship award, and NanoInjection Technologies, LLC.

I am indebted to Brigham Young University, the faculty and staff for the education I have received in helping me grow intellectually and learn spiritually. I feel a deep sense of gratitude toward Dr. Brian Jensen who accepted me as a prospective doctoral student and always encouraged me along the way. I have thoroughly enjoyed working with him and have a great admiration for him. I am grateful to the rest of my committee members for their support, Dr. Ken Chase and Dr. Aaron Hawkins, especially Dr. Sandra Burnett for her expertise in Micro-biology and Dr. Larry Howell for his insights and comments.

Justin L. Black has been extremely useful in helping with all of my experiments. Special thanks to Quentin T. Aten for his prior research that led to this work.

My parents have always been an immense influence in my scholastic pursuit. They have provided a way for me to be educated and for that I am forever grateful. They have always been supportive in my choices. I love them and I am grateful for their love and support.

I would like to recognize my wife for all that she does for our family, for her devotion, love, and support toward me, without whom I could not have done any of this.

Finally, I need to recognized the tender mercies of GOD in my life. “In nothing doth man offend God, or against none is his wrath kindled, save those who confess not his hand in all things, and obey not his commandments.” (D&C 59:21.)

TABLE OF CONTENTS

LIST OF TABLES

LIST OF FIGURES

NOMENCLATURE

DNA	Deoxyribonucleic acid
PBS	Phosphate buffered saline
EDTA	Ethylenediaminetetraacetic acid
MEMS	Microelectromechanical systems
TRITC	Tetramethyl Rhodamine Isothiocyanate
RFP	Red Florescent Protein
TAE	Tris-acetate-EDTA (buffer solution)
EtBr	Ethidium bromide
BEM	Boundary Element Method
hCG	human chorionic gonadotropin

CHAPTER 1. INTRODUCTION

1.1 Motivation

Microinjection is the process of using a very fine needle to insert foreign microscopic matter, i.e. DNA, into a single living cell. This allows the new substance to become part of the reproduced genetic material to create organisms that exhibit additional, enhanced, or repressed genetic traits [1, 2]. Even though microinjection has been extensively used for biological studies for the last 50 years, the basic approach (injecting desired contents through a microneedle) has not changed since its introduction. The initial development of an automated MEMS-based lab-on-a-chip nanoinjector as shown in Figure 1.1 was recently developed at Brigham Young University [3]. MEMS-based lab-on-a-chip (Micro Electromechanical Systems) refers to the integration of mechanical components, sensors, actuators, and electronics on a common silicon substrate through microfabrication technology. This innovative approach emphasizes the pumpless, solid design of the needle referred to as a lance. Instead of using macro-scale pumps to force DNA into the cell, nanoinjection uses electrical forces to attract DNA to the solid lance and after puncturing the cell with the lance, repelling the attracted DNA using electrical forces. Figure 1.2 is a side view schematic representation of Figure 1.1. One terminal of the voltage source is connected to the lance and the other is connected to the monosilicon substrate of the MEMS die. In comparison to microinjection, the nanoinjector has the benefit of not introducing measurable amounts of extraneous liquid into a cell causing genomic damage [3].

1.2 Problem Statement

Accurately predicting DNA motion is crucial for nanoinjection. To further nanoinjection development, I extend the research by developing a mathematical model accurately predicting the motion (trajectory) of DNA during the nanoinjection process. This mathematical model will

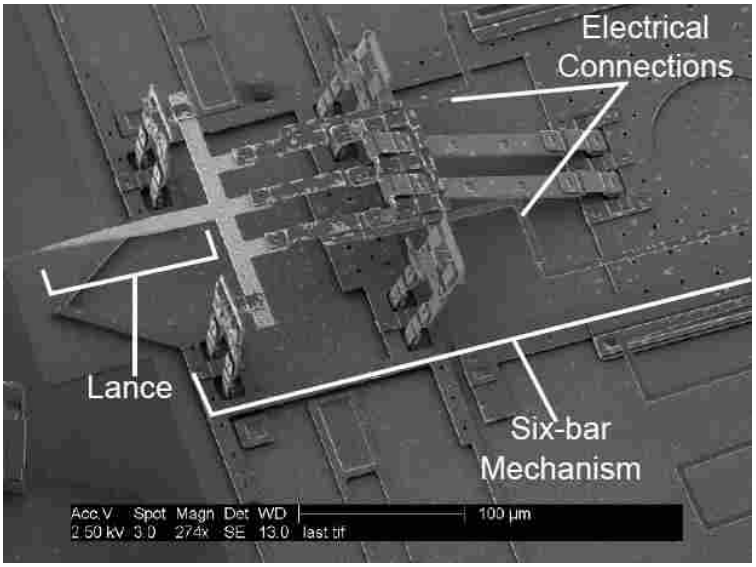

Figure 1.1: Scanning electron micrograph of the MEMS lance assembly in its deployed position 50 μm above the substrate of the MEMS die.

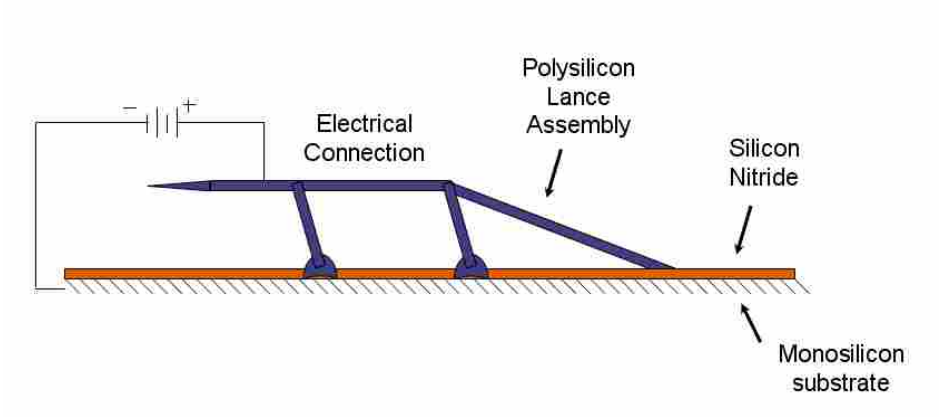

Figure 1.2: Diagram of the electrical connections used to apply voltage during DNA attraction and repulsion of the lance

help determine and quantify the significant parameters affecting nanoinjection. To validate the mathematical model, visual experimental evaluation of the motion of DNA due to the local electric fields is studied. First, DNA motion is studied in saline solution between two stainless steel parallel plates. Second, the effects of dissimilar electrode material (silicon and steel) on DNA motion are examined. After experimental verification of the model, a comparison study of design parameters is conducted to identify ways to improve the efficiency of nanoinjection.

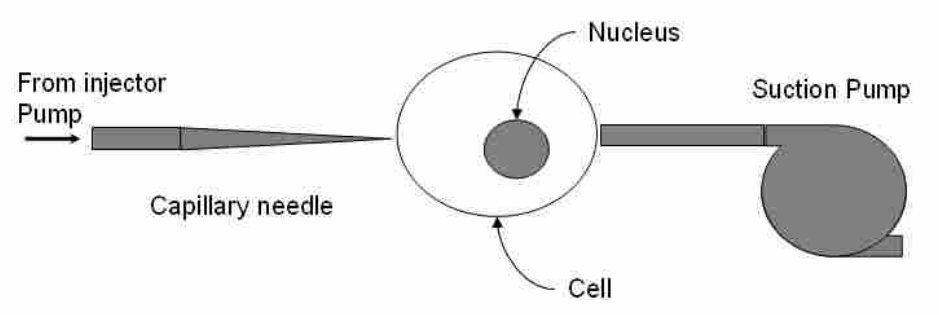

Figure 1.3: A schematic representation of a typical microinjection

To show the previous work that is drawn upon for this research, background in the proposed area is given as a literature review. After this developmental background is given, a detailed description of the research objectives is presented. Finally, a listing of contributions is presented, including publications.

1.3 Background

To fully understand the scope of research and the knowledge and research already developed, a brief background is given. This background discusses preliminary development and data on the pumpless MEMS nanoinjector and a brief discussion on the nature of electrical forces, and its application to this research.

1.3.1 Pumpless MEMS Nanoinjector vs. Microinjector

A microinjector is a device used for microinjection. It consists of a very fine, drawn glass capilarry needle used to puncture the outside and/or the nuclear membrane of a cell and to channel the fluid containing the foreign microscopic matter. Micro fluidic pumps are used to deliver precise amounts of genetic material into the cell as reported by [2].

Figure 1.3 illustrate a cell undergoing microinjection. Recent work on microinjection has shown that the physical process of microinjection, specifically the injection of extracellular fluids, damages the target cell chromosomes and may be a principal contributor to decreased embryo viability following microinjection [3,4]. Dramatic developmental changes and/or cell death is typically observed in 20 to 50% of microinjected embryos [1,2,4,5]. In efforts to limit the damaging

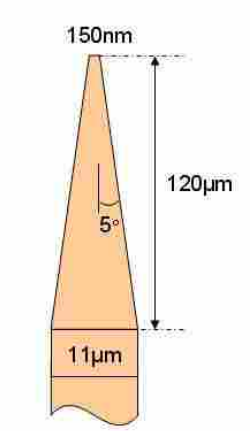

Figure 1.4: Dimensions for the tip of the lance used in nanoinjection

effects of microinjection, recent research has produced even finer, smaller microinjection needles than drawn capillaries from silicon nitride [6] or silica glass [7]. However, these needles employ macro-scale pumps similar to those used in traditional microinjectors.

The central element of nanoinjection is a lance which electrically attracts DNA to its outer surface, pierce the cellular membrane of a cell, electrically repels DNA off its outer surface and into the cell and finally retracts from the cell [3]. Prototype MEMS lances were fabricated using the polyMUMPs fabrication technology, which provides for two structural layers (2.0 μm and 1.5 μm thick respectively) and a gold layer [8]. A prototype MEMS lance is shown in Figure 1.1.

The lance shown in Figure 1.1 consists of a solid, tapered body having a nominal thickness of 2 μm, and a minimum tip width of 150 nm as shown in Figure 1.4. The lance is 120 μm long and tapers at a 10° angle to a maximum width of 11 μm [3].

1.3.2 Electrical Force

The pumpless MEMS lance operates on the principle of attraction and repulsion of DNA using electrical charges. Charged particles such as DNA, proteins and peptides, experience forces when placed either in a uniform or non-uniform electrical field, as illustrated in Figure 1.5.

The pumpless nanoinjector is made feasible by the unequal charge distributions within DNA molecules. The phosphate backbone of the DNA has a net charge of one electron per phosphate, giving a total of two electrons per base pair [9]. This net negative charge on the outer

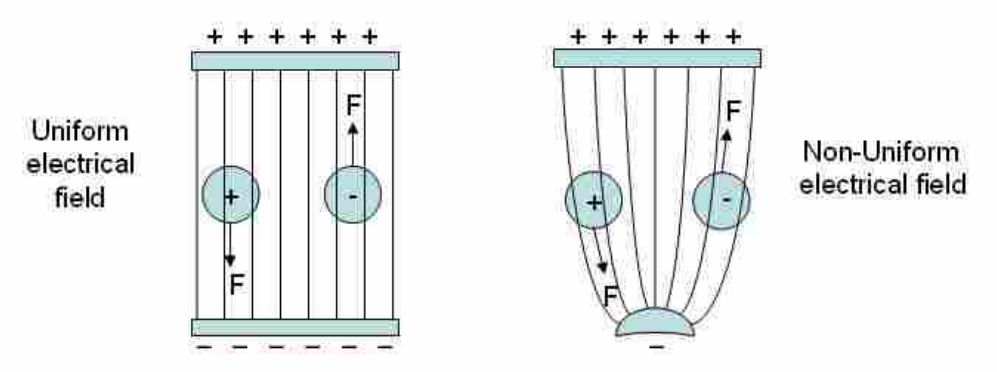

Figure 1.5: Electrophoresis forces on charged particles

backbone of the DNA makes it possible to move DNA from one point to another using the electric field generated by charges. These forces are useful for transportation, separation and characterization of bioparticles [10]. This phenomenon is called electrophoresis. The Greek word phoresis, meaning motion, is part of the root of the term 'electrophoresis' that implies the study of motion for small biological organisms [11].

Electrophoresis has been used to separate living and dead cells, distinguish the normalcy of blood cells and characterize the cell aging process [12]. It has also been applied to microfuidic devices to characterize or to physically trap biological cells or particles [13, 14]. Microfabricated devices using this approach with integrated chemical reaction stages have been fabricated [15]. In 1994, a molecular motion analysis of protein and DNA was investigated in which a biopolymer solution was moved through a high-intensity field region created in a fluid integrated circuit, and the polymer was analyzed and / or separated [16]. The electrical manipulation of nanoparticles using nonuniform electric fields has proved a useful method of investigating the movement of charge around colloidal particles [17]. Other research has shown that this method can also be used to position the DNA and proteins at well-defined positions on a chip [18]. Electric fields move DNA several inches through agarose or polyacrylamide gels during macro-scale electrophoresis experiments [19, 20]. Similarly, on the MEMS scale, researchers have used electric fields to perform electrophoresis in microcapillaries [21], and to move nanoliter drops of DNA through a self contained DNA analysis system [22]. Finally, in work at BYU, sufficient amount of DNA to transfect a cell was attracted to and repulsed from a conductor using an electrical field [3].

1.3.3 Electrophoresis Models

Models designed to predict the motion of particles (i.e. DNA) in gel electrophoresis have been studied, developed and published as an attempt to better understand the underlying physical principles. These models are categorized into two groups. The first is a statistical model group, some using Brownian motion from diffusion constants and thermal energy [23, 24], others comparing binomial distribution to poisson distribution effects [25]. The second model group relates particle mobility to electric field strength [26], DNA concentration [27], friction coefficient [28], and different particle shapes [29]. Some models also have combined the interaction between electric energy and thermal energy [30, 31].

These previous models all treat the electric field as constant and nonuniform, which is an appropriate assumption for most prior electrophoresis. However, in the DNA manipulation scheme being developed in our lab, the electric field is neither constant or uniform. Therefore, we propose to develop a model with the following characteristics. First, the model will be time dependent. It will use a set of dynamic equations to describe the motion and position of particles (i.e. DNA), as well as the electric field, as a function of time. Second, the model will calculate the electric field from the geometry and the voltage on the electrodes. This will allow us to look at the effects of non-uniform electric fields. Third, the model will be dependent on the concentration, the viscosity and the dielectric constant of the solution as well as the size of the particle (i.e. DNA). Fourth, the model will be generalized to predict singular or interactive bulk attractive or repulsive motion given physical boundary constraints.

1.4 Approach

Figure 1.6 shows the electrical connections that provide an electrical path between the lance and the substrate as shown on Figure 1.1. One terminal of the voltage source is connected to the lance and the other is connected to the monosilicon substrate of the MEMS die. When a potential voltage exists between the two electrodes, charges will collect on the surface of the conductor, creating an electric field around the lance. The model predicts the electric behavior around the lance due to the potential difference between the lance and the ground electrode. No exact closed-form solution is available for the complex geometry; therefore, a numerical solution is

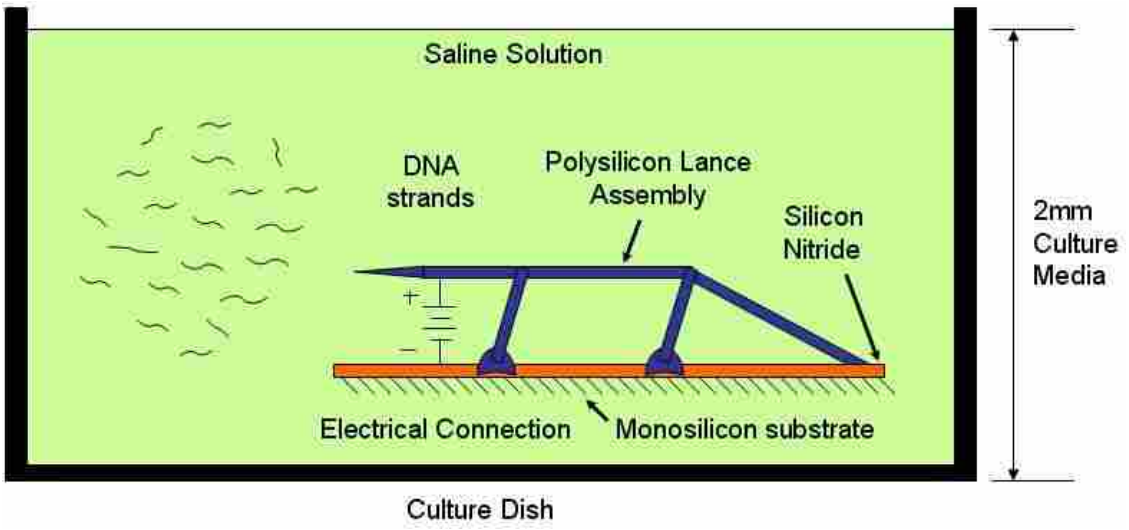

Figure 1.6: Diagram of the electrical connections used to apply voltage during DNA attraction and repulsion of the lance

developed. The Boundary Element Method (BEM) is used to calculate the charge density on each electrode. The resulting charge distribution collected on the surfaces of the conductors is then used to calculate the electric field. The model then predicts the macromolecular motion of DNA due to the electric field created from the charges on the surfaces of the conductors. An applied electric force, a viscous resistive force, and an electrophoretic retardation force are considered to act on a DNA particle. The sum of the forces defines the acceleration of the particle. The position and velocity can then be determined from the acceleration. The model is to be verified and validated against experimental results. In addition, it will be shown that the model accurately predicts large curved-field motion of charged particles in the presence of a non-uniform electric field created by similar or dissimilar electrodes.

1.5 Research Objectives

The proposed research can be categorized in the following five objectives.

- Create an analytical model capable of predicting the electric field around complex geometry (vicinity of the lance) and model the macromolecular motion (attraction and repulsion) due to the electric field.

- Experimentally evaluate the DNA motion as a function of time, under electrical forces. This step helps to visualize DNA motion and allow validation of the modeling. DNA motion in saline solution is studied between stainless steel parallel plates. These experiments validate the model.

- To further extend our understanding of DNA motion for the nanoinjector, experimentally observe and predict (with model) large curved field motion of charged particles during electrophoresis and study the effects of dissimilar electrode material (steel and silicon) on decomposition voltage, electric field and DNA motion.

- Using the model, perform a comparison study of design parameters to identify ways to improve the efficiency of nanoinjection.

- Include a study of the electric field strength sufficient to cause localized electroporation to facilitate DNA transfer to the pronucleus.

1.6 Contributions

The pumpless MEMS lance represents an important and significant step in the development of a self-contained, automated, MEMS-based cell injection system. The pumpless MEMS lance operates on the principle of attraction and repulsion of DNA using electrical charges. Accurate prediction of the displacements of the DNA after repulsion within the cell is very important. This research demonstrates the feasibility of this technology, including a predictive dynamic model. The implementation of the model is compared and validated with experimental data. The model is finally used to investigate the effects several parameters have on DNA motion. This work lead to at least three journal publications. One paper focuses on the modeling and experimental validation of DNA motion in uniform and non-uniform DC electric fields. This paper has been accepted for publication to the ASME *Journal of Nanotechnology in Engineering and Medicine* [32]. Another describes the effects of dissimilar electrode material on DNA motion during electrophoresis. Finally, the third is a comparison study of design parameters to identify ways to improve the efficiency of nanoinjection. A fourth paper is planned to describe both modeling and experimental testing of localized electroporation, with the modeling coming from these results.

CHAPTER 2. MODELING AND EXPERIMENTAL VALIDATION OF DNA MOTION IN UNIFORM AND NON-UNIFORM DC ELECTRIC FIELDS [1]

2.1 Introduction

Recently, our group has begun the development of an automated MEMS-based lab-on-a-chip system for DNA injection [33]. Our approach uses electrical forces to move DNA. The phenomenon of moving DNA using an electric field is called electrophoresis. We have developed a mathematical model describing the motion of DNA in response to electric fields. The model will be useful to improve our understanding of DNA motion conditions related our new possible approach for creating transgenic animals.

The purpose of this chapter is to describe the experimental setup for DNA motion, report experimental results, present the mathematical model with assumptions and theory, and validate the model by comparing the experimental results to the model predictions.

2.1.1 Electrophoresis Background

Charged particles such as DNA, proteins, and peptides experience forces when placed in an electrical field. The pumpless microneedle is made feasible by the unequal charge distributions within DNA molecules. The phosphate backbone of the DNA has a net charge of one electron per phosphate, giving a total of two electrons per base pair [9]. The net negative charge on the outer backbone of the DNA makes it possible to move DNA from one point to another using the electric field generated by electrical charges. This phenomenon is called electrophoresis. Electrophoresis is commonly used for transportation, separation and characterization of bioparticles [34, 35]. It has also been applied to microfluidic devices to characterize or to physically trap biological cells or particles [13, 14].

[1] This chapter has been accepted for publication to the *Journal of Nanotechnology in Engineering and Medicine* [32].

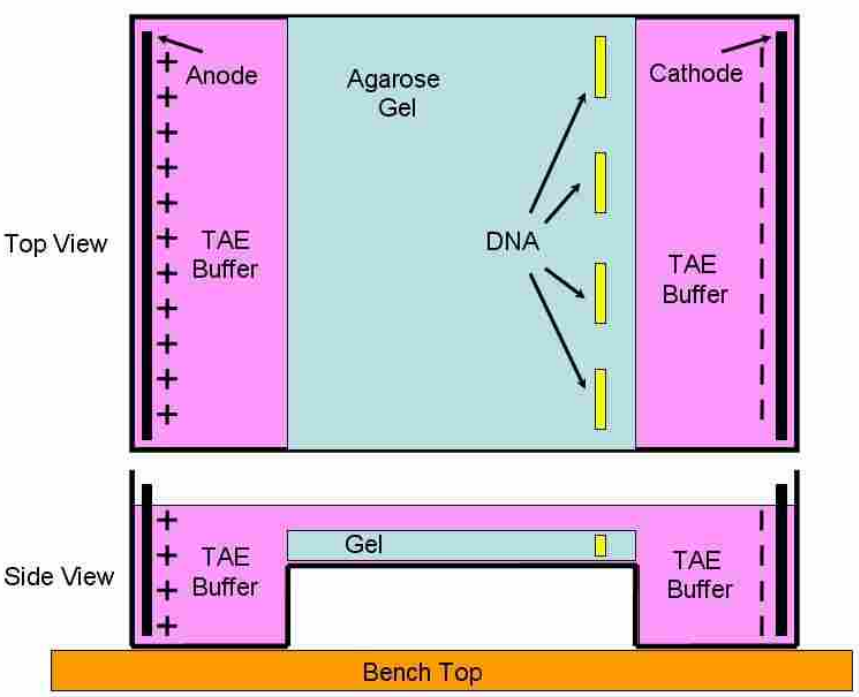

Figure 2.1: A schematic representation of a typical gel electrophoresis

Gel electrophoresis is a process used to separate/move DNA, RNA or protein molecules through a gel matrix using an electric field. Figure 2.1 represents a simplified gel electrophoresis device. The device consists of a container where the gel, the buffer solution, and the electrodes are placed. A comb is placed in the gel mixture to form grooves. Once the gel has solidified, more ionic solution (buffer solution) is poured into the container. The gel is now bathing in ionic solution. The comb is removed and a mixture of DNA with a loading dye is placed in the grooves. The electrodes are placed and a potential difference is applied to create the electric field. The DNA, being negatively charged [9], will be repelled by the cathode and attracted to the anode.

2.1.2 Microscope Imaging

After electrophoresis is completed, the molecules in the gel can be stained to make them visible. A dye is usually used for staining [3]. Ethidium bromide (EtBr) is a fluorescent dye which intercalates between the stacked bases of DNA. EtBr is commonly used to stain double-stranded DNA separated in agarose gels. The advantage of this stain is that one can observe the

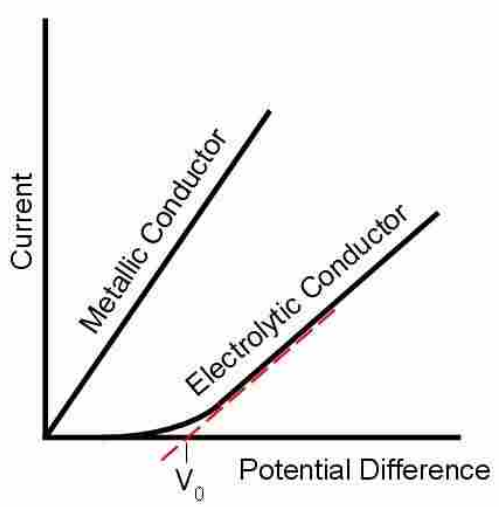

Figure 2.2: Ohm's law in metallic conductors and in electrolytes

separation directly by viewing the gel under a microscope with the correct filtered light during the electrophoretic process. The DNA is stained prior to electrophoresis [36].

2.1.3 Electric Current Conductors

Figure 2.2 shows typical voltage-current curves for two general types of electrical conductors, metallic conductors and electrolytic conductors. The current conduction in metals or graphite is based on transport of electrons through the conductor. For solutions of acids, bases or salts (electrolytes), the conduction is due to a transport of ions (anions and cations). In the presence of an electric field, the cations move toward the negative electrode while the anions move towards the positive electrode. Notice that for an electrolytic conductor, the current flows appreciably only above a certain value denoted as the decomposition voltage V_0 [37].

Ohm's law above the decomposition voltage in an electrolyte may be approximated as

$$I = \frac{E - V_0}{R} \tag{2.1}$$

where I is the current in amperes, E is the potential difference between the two electrodes in volts and V_0 the decomposition voltage also in volts.

An ionic solution is necessary for electrophoresis. In the presence of a poorly conductive medium (i.e. deionized water), the few positive and negative ions present will move toward the an-

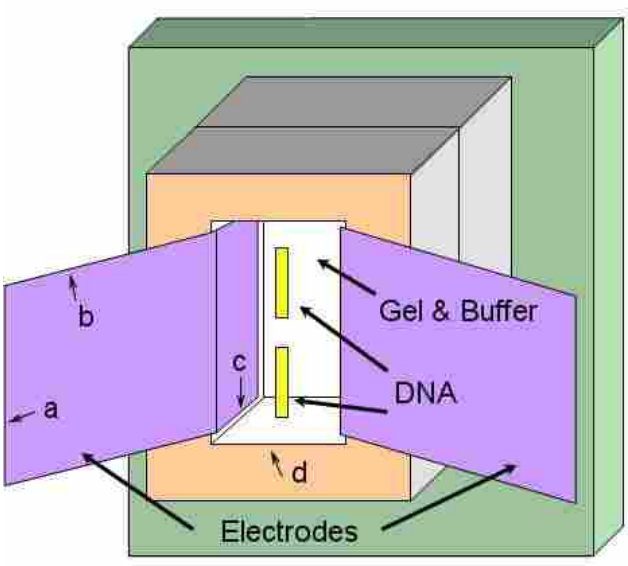

Figure 2.3: Schematic macro size gel electrophoresis device

ode and cathode mitigating the effect of the electric field between the electrodes [38]. This means that a charged particle placed between the two electrodes will not move much under electrostatic forces. In contrast, in a conductive medium (one with plenty of ions) an electrical circuit is completed and current is allowed to flow, assuming that the voltage is above the decomposition voltage. The electrical current allows for significant motion of charged particles.

2.2 Methods

2.2.1 Experimental Setup

Gel Electrophoresis Setup

Figure 2.3 represents a schematic version of the gel electrophoresis device used for the experiments. The device is made from 3 acrylic layers (a base, a bottom and a top layer). The base is 48 by 48 by 6 mm solid acrylic. The bottom layer is 22 by 11 by 3.12 mm solid acrylic. The top layer is identical to the bottom layer except it has a cut out section (11 by 7 mm) to hold the gel and position the electrodes.

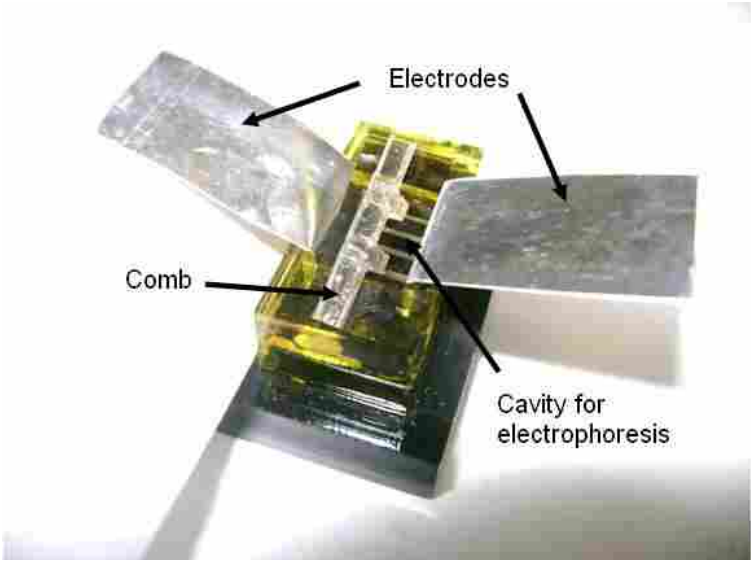

Figure 2.4: Photograph of experimental device

Table 2.1: Parameters and values found in Figure 2.3

Parameter	**Value (mm)**
a	10.63
b	17.88
c	3.12
d	6.37

The electrodes are made from stainless steel to reduce corrosion and discharge during electrophoresis. The parameters a, b, c and d found in Figure 2.3 describe the dimensions of the electrodes and the gap between the electrodes. Their values are noted in Table 2.1.

The electrodes extend through both the top and bottom acrylic layers, so the total length of the electrode is 24.12 mm. The thickness of each electrode is 0.15 mm and they are positioned 6.37 mm apart. The device is assembled using acrylic glue. Figure 2.4 is an image of the actual device used for the experiments. Placed within the device is the acrylic comb used to create the grooves for the DNA.

To see how adaptable the mathematical model is to different electrode configurations (other than parallel plates), the experiment shown in Figure 2.5 is conducted. Two thin steel electrodes (width of 2.7 mm) are placed at an offset diagonal of each other (2 cm horizontally and 1.75 cm

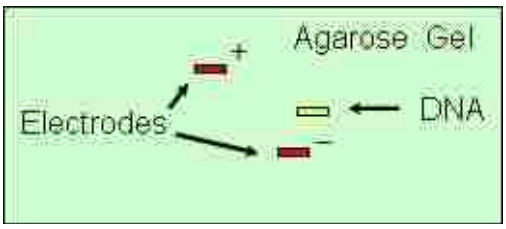

Figure 2.5: Testing the effects of electrode configuration on DNA motion

vertically). DNA is placed in between the electrode, 1 cm from the bottom electrode. The set up uses a 9 cm by 7.5 cm box where the gel is cooled.

Experimental Protocol Description

Experiments were performed to measure the velocity of DNA motion through an electrolytic solution as a function of voltage. Data for these experiments were obtained using the following experimental setup.

The ionic solution through which DNA movement was measured is composed of agarose (30 mg), and phosphate buffered saline (PBS, an isotonic buffer solution - 10 ml). Traditionally, TAE (Tris-acetate-EDTA) is used during electrophoresis. Because PBS is the buffer solution used during the MEMS-based injections, we will study its effect on DNA motion first. TAE results will be presented towards the end of this chapter.

The gel was prepared by first measuring the appropriate volume of PBS using a graduated cylinder. The agarose powder was then measured using a scale and the two ingredients were mixed together in a small Erlenmeyer flask. The solution was heated to boiling in a microwave, then mixed by swirling. The boiling and mixing was repeated two more times after which the solution was allowed to cool. For a 10 ml gel, 0.4 μl of ethidium bromide was added using a micropipette and the solution was stirred again. As the solution cooled to room temperature, it began to thicken into a viscous liquid. Approximately 400 μl of the solution was needed for the device shown in Figure 2.4.

With the stainless steel plates connected to a power supply, DNA was added to the solution by micropipetting 3 μl of DNA (34 ng/μl) into only one of the grooves. DNA strands (4699 basepair) diluted in PBS are used for these experiments. After adding DNA, the device was placed

Table 2.2: Voltage used for each experiment on each day

	Voltage For Experiments (V)					
Day 1	0	1.5	3	4	5	-
Day 2	1.5	3	4	5	6	-
Day 3	2.5	3	3.5	4	4.5	5

under a fluorescent microscope (Zeiss Imager A.1 with a 12 megapixel digital camera) to image the DNA. UV light was supplied to the microscope through a TRITC-A/RFP (red fluorescent protein) filter using an X Cite fluorescence lamp. The computer software used to save and manipulate the images is Axiovision 4.8.

Experiments and Current vs Voltage Curve for PBS Gel Electrophoresis

Experiments were carried out over 3 days using both devices. Table 2.2 describes the voltages used for each experiment conducted on all 3 days.

The voltages were selected as follows:

- 0 V: the control experiment for comparison with other voltage levels.
- 1.5 V: A voltage between 0 V and the decomposition voltage.
- 2.5-6 V: higher voltages used to investigate their effect on DNA motion.

In addition to the experiments performed on DNA motion, an experimental current-voltage curve was extracted to determine the decomposition voltage for the ionic solution used in the experiments. According to data (Figure 2.6), the decomposition voltage for agarose/PBS is 2.94 V.

Data Analysis

When exposed to ultraviolet light, ethidium bromide will fluoresce. When bound to DNA, it will fluoresce up to 20 times brighter [36]. Under the microscope, the DNA bound by EtBr appears in solution as a fluorescent cloud. Once the DNA is located, an image is taken which represents time 0 seconds. Voltage is then applied to the device using the power supply. The left electrode on the device is positive and the right electrode is negative. For the experiments and images, the

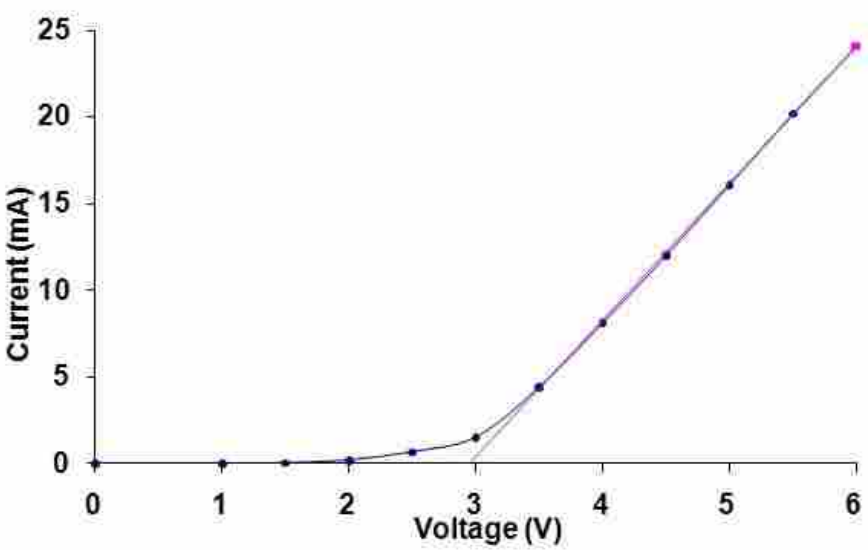

Figure 2.6: Effects of voltage on current in 30mg agarose/10ml PBS

DNA is thus expected to move from right to left. Images are subsequently taken between recorded intervals and movement of DNA is observed as the fluorescent cloud moves from the negative electrode to the positive electrode.

MATLAB is used as the postprocessor to analyze pixel motion within each image saved. This way each image is compared to a reference image to track motion. The reference image is the first image saved at time 0 with no voltage. Using the reference image, one very small group of hand selected pixels(from one area of the image where the color change is very visible) is chosen. This will allow the user to obtain a numerical value representing an average of the color intensity selected. That value can then be traced in each successive image for that experiment. This can only be done accurately as long as every image during one experiment is the same size and the object imaged is stationary in time. Once the pixel count for the estimated motion is established, the displacement is calculated using a calibration for a pixel size. For all experiments, the calibration is 0.33 μm per pixel and the estimated displaced measurement error is ± 20 μm per image.

2.2.2 Mathematical Model

The model developed here is designed to work for any geometry of electrodes placed in an electrolytic solution. When a potential voltage exists between the two connections, charges will

collect on the surface of the conductors, creating an electric field around them. The mathematical model predicts the resulting charge distribution and the electric field around the parallel plates. It will then predict the motion of DNA molecules in the field.

Modeling the Surface Charge Density

The electrodes shown in Figure 2.3 act as two parallel electrodes, each with identical geometry. When a voltage exists between the electrodes, charges will collect on the surface of the conductors, creating an electric field. The boundary element method is used to solve for the surface charge density on the boundary of each electrode. Assuming that the electrode resistance is very small compared to the electrolyte resistance, the charges can be modeled using the poisson equation

$$\nabla^2 V = -\frac{\rho_v}{\varepsilon} \tag{2.2}$$

where V is the voltage, ρ_v is the volumetric charge density and ε is the permittivity of the medium.

Equation (2.2) may be written in the form of the Kirchoff integral equation

$$V(r) = \frac{1}{4\pi\varepsilon} \int\int_S \rho_s(r') \left[\frac{1}{|r-r'|}\right] dS' - \frac{\rho_v}{\varepsilon} \tag{2.3}$$

where ε is the permittivity of the medium, r is the testing point (the point at which the voltage is predicted) and r' is the integration point (the point at which the differential area dS' is integrated). ρ_s is the surface charge density and S is the boundary surface to the domain of interest. For parallel plates, simplifying assumptions could be made to allow equation (2.3) to be solved analytically. However, to retain generalization of the model for any geometry, we chose to solve equation (2.3) using the boundary element method.

In the boundary element method, the underlying equations describing a system are converted into the form of an integral equation. Instead of attempting to integrate the resulting equations over a complex domain or boundary, the problems are discretized by dividing the domain into a large number of similarly-shaped pieces, termed elements. The creation of these elements, known as 'meshing' the domain (the surface of the conductors), converts the problem from a single, nearly intractable problem into a large number of related but relatively simple problems, allowing

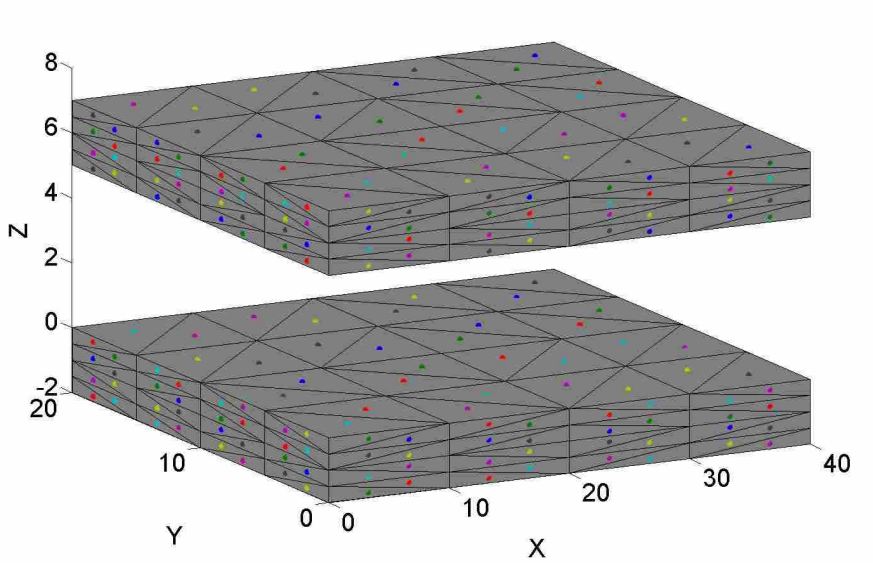

Figure 2.7: Illustration of geometry, mesh and point charge at the centroid of each triangular mesh element

an approximate solution to be calculated using a computer. Triangular elements are used to mesh the geometry. The solution to the boundary element method gives the charge density for each triangular element [39]. The charge density can then be approximated as a single point charge acting at the centroid of the triangular elements.

We implemented the three-dimensional boundary element solution to equation (2.3) in MATLAB, and used it to solve for the charge density on both conductors. Figure 2.7 shows an example illustrating the mesh and the point charge at the centroid of each triangular mesh element for two parallel electrodes.

Because the volumetric charge density from each DNA particle (ρ_v in Equation (2.2)) is a function of position, the charge density on the conductor will need to be recalculated every time the DNA particles move in addition to calculating their trajectories [40–42].

Nanoinjection takes place in a saline solution conducive to cell survival. The dielectric constant of saline water has been studied extensively [43–48]. For a temperature of 25 $^\circ$ Celsius (room temperature) and a salinity of 0.9%, the estimated low-frequency dielectric constant of the solution is 75.07, resulting in a total permittivity of 6.647×10^{-10} F/m.

Electric Field Calculation

An electric field is said to exist in the region of space around a charged object. In the presence of more than one charged object, the total electric field at any point P equals the vector sum of the electric fields of the individual charges,

$$\mathbf{E_p} = \frac{1}{4\pi\varepsilon}\sum \frac{q_i}{{r_i}^2}\hat{\mathbf{r}}_\mathbf{i} \tag{2.4}$$

where r is distance from the ith charge q_i to the point P and $\hat{\mathbf{r}}_\mathbf{i}$ is a unit vector directed from q_i toward P. Given the charges located on the conductors and the position of the DNA molecules, equation (2.4) can be used to numerically calculate the magnitude of the electric field.

Particle Dynamics

The dominant factor for motion of the DNA will be the electrical force exerted on a molecule due to the electric field present resulting from the charges on the conductors. The force applied on a particle of charge q and mass m within the electrical field $\mathbf{E}$ is given by

$$\mathbf{F_{applied}} = \mathbf{E}\, q \tag{2.5}$$

The electric force described in equation (2.5) will cause the particle to accelerate. Increasing the velocity of the particle is then balanced by an increasing viscous drag. When the viscous force balances the applied electric force, the particle moves with a steady velocity. Recent research has shown that the motion of a DNA fragment within the presence of an electrical field can be modeled using Coulomb force and Stokes's law for hydrodynamic drag force [49]. DNA fragments were assumed to be "prolate spheroids" with a variable sphere radius equivalent in volume to the volume occupied by the sum of each DNA base pair modeled as a cylinder. Stokes showed that the viscous drag on a sphere is proportional to the velocity of the particle. The drag force is $6\pi\eta av$ where η is the fluid viscosity, a is the particle radius and v is the particle velocity [50,51]. A third force called electrophoretic retardation [52] results from the presence of the small electrolyte ions in the solution. This force is defined by

$$F_{ions} = (q - \varepsilon\zeta a)\mathbf{E} \tag{2.6}$$

where a is the radius of the particle, q is the charge of the particle, E is the electric field, ζ is the electrokinetic (or zeta) potential and ε is the dielectric constant. ζ is defined as

$$\zeta = \frac{q}{\varepsilon a(1+\kappa a)} \tag{2.7}$$

where κ is the reciprocal of the thickness of the double layer [37, 53]. The double layer thickness is a measure of the ionic concentration present in the solution. It is defined by the following points: 1000 Å for a 10^{-5} M solution, 100 Å for a 10^{-3} M solution, 10 Å for a 10^{-1} M solution and 1 Å for a 10^{1} M solution [54, 55].

The total force on the particle subject to an applied electric force in an electrolytic solution is represented by

$$\mathbf{F_{total}} = \mathbf{E}\, q - 6\pi\eta a\mathbf{v} - (q - \varepsilon\zeta a)\mathbf{E} \tag{2.8}$$

Newton's second law, combined with equation (2.8) gives

$$\mathbf{F_{total}} = m\frac{dv}{dt} = \mathbf{E}\,(\varepsilon\zeta a) - 6\pi\eta a\mathbf{v} \tag{2.9}$$

where t is time. Equation (2.9) can then be applied to the particle to determine its acceleration (magnitude and direction) under the force caused by the electric field, the viscous force, and the ionic concentration of the electrolytic solution. Integrating the acceleration as a function of time will define the velocity (first integration) and position (second integration) of the particle. Because of the nature of the integration, one initial condition needs to be specified to define the velocity and another initial condition for the position of the particle.

Trajectory

In order to obtain a solution to equation (2.9), a numerical integration is performed using the ODE15s solver in MATLAB. ODE15s is a general purpose solver appropriate for a wide variety of initial value problems. The electric field at each point represented in equation (2.5) is a function

of all three spatial coordinates (x, y, and z). This in turn indicates that the acceleration, velocity and position of a particle will also be a function of all three spatial coordinates (x, y, and z). The state equations that will yield the velocity and the position of a particle are separated into components and represented by equations (2.10 - 2.15) below:

$$\dot{\delta}_x = v_x \tag{2.10}$$

$$\dot{v_x} = \frac{E_x\,(\varepsilon\zeta a) - 6\pi\eta a\, v_x}{m} \tag{2.11}$$

$$\dot{\delta}_y = v_y \tag{2.12}$$

$$\dot{v_y} = \frac{E_y\,(\varepsilon\zeta a) - 6\pi\eta a\, v_y}{m} \tag{2.13}$$

$$\dot{\delta}_z = v_z \tag{2.14}$$

$$\dot{v_z} = \frac{E_z\,(\varepsilon\zeta a) - 6\pi\eta a\, v_z}{m} \tag{2.15}$$

Geometry and Parameters

The geometry for the theoretical model is loaded to reflect the dimensions found in Figure 2.3 or Figure 2.5. In addition to the geometry, the double layer thickness and the zeta potential must be calculated. The ionic concentration for PBS is 0.1514 M, returning a value of 8.1 Å for the double layer thickness and a zeta potential of 5.8 V. This zeta potential effect reduces the effective charge of the particle from 0.0015 pC to 6.72×10^{-5} pC (for a 4699 basepair DNA molecule weighing 5.1×10^{-9} ng with an effective drag radius of 17.4 nm).

Because the decomposition voltage is set at 2.94 V (the potential at which significant current flows) as illustrated in Figure 2.6, the mathematical model is established to predict displacements only for values above V_0. Thus the voltage used in predicting the electric field is established by

$$V = V_{Applied} - V_0 \tag{2.16}$$

Finally, the viscosity of the gel is updated. Measurements using a viscometer reveals that the gel is between 30 and 50 times more viscous than water at room temperature. (As a point of

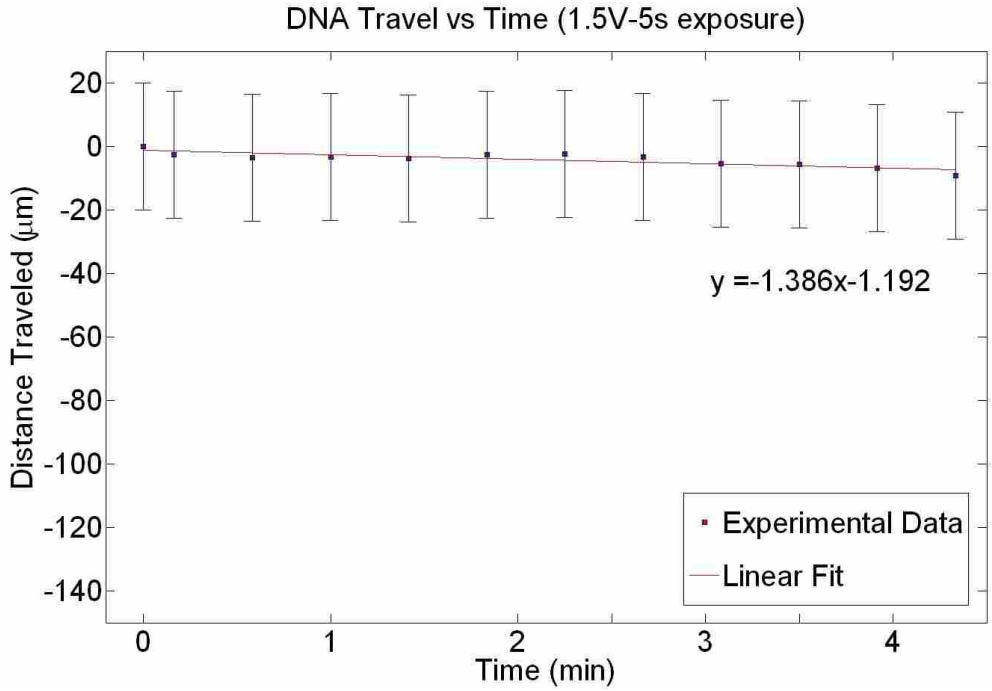

Figure 2.8: DNA motion for each image for the experiment conducted at 1.5 V on day 2. The estimated displaced measurement error bars are added. Compare with Figure 2.9. The velocity is indistinguishable from zero at this voltage.

reference, the viscosity of olive oil is 90 times that of water at room temperature.) The viscosity is set at 0.0340 N·s/m^2.

2.3 Results

2.3.1 Experimental Results

At 0 V or voltage well below the decomposition voltage (2.94 V), the DNA should only move due to diffusion since the electrostatic forces are negligible. Figure 2.8 shows the motion of DNA for every image taken within 260 seconds for the experiment conducted at 1.5 V on day 2. Average DNA velocity is approximated using the slope of a least squares line. At 1.5 V, on average, the DNA has traveled 1.3 μm per minute. Because the measurement uncertainty is larger than the total measured displacement, the data confirms that the DNA velocity at 1.5 V is indistinguishable from zero.

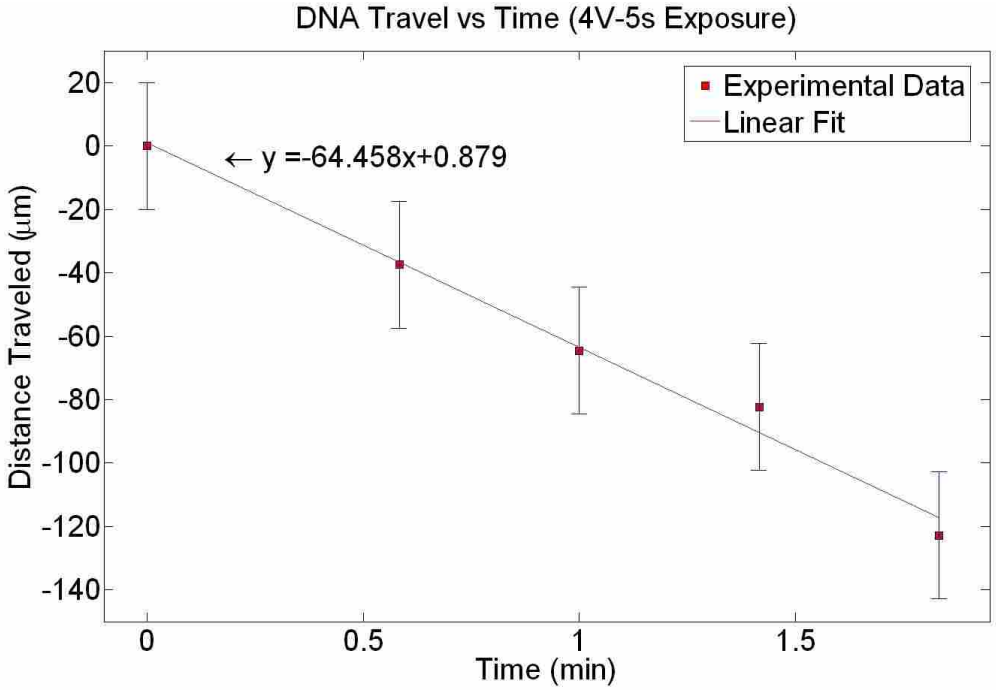

Figure 2.9: DNA motion for each image for the experiment conducted at 4 V on day 2. The estimated displaced measurement error bars are added.

Each experiment used equal amounts of DNA but varied by the amount of voltage applied to the device. Similar to Figure 2.8, Figure 2.9 represents the results of the experiment conducted at 4 V on day 2. The time for the experiment has significantly been reduced from 260 to 110 seconds and the DNA has traveled 64.45 μm per minute.

The average DNA velocity was determined for all experiments defined in Table 2.2 and the resulting measured DNA velocities are shown as a function of voltage in Figure 2.10. Figure 2.10 also shows the least-squares line fit to the data above 3.5 V and the model prediction.

2.3.2 Modeling Results

With the above described effects included and the parameters and the geometry updated, four simulations were analyzed. For each simulation (3, 4, 5 and 6 V), the same input coordinates for the DNA particles were specified. All other parameters were set equal to those used for the experimental data shown in Figure 2.10, as described above.

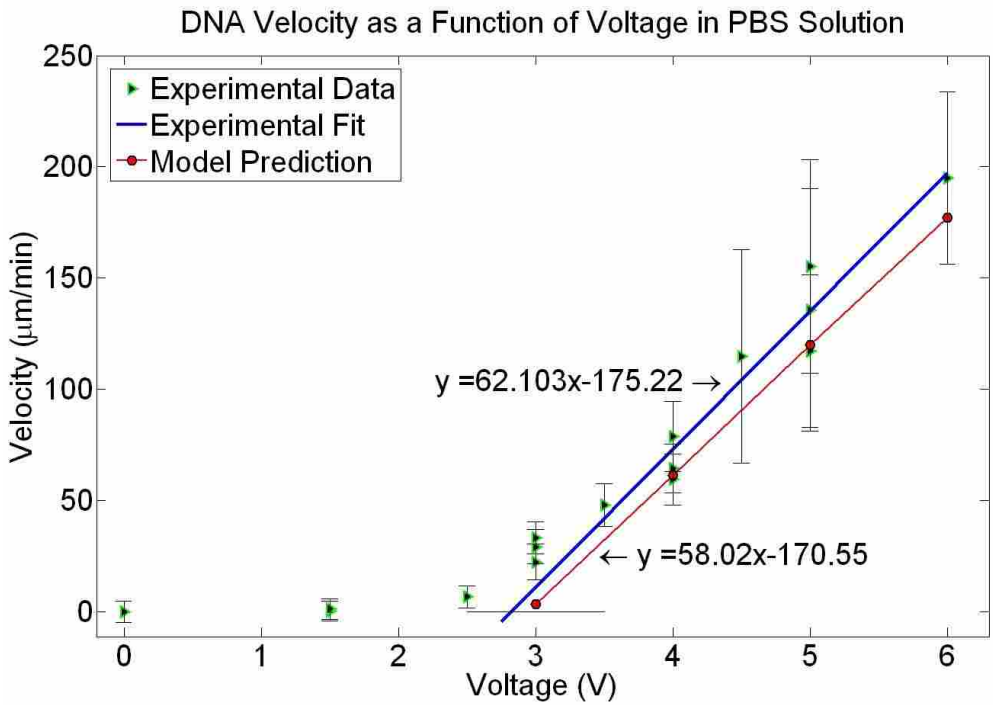

Figure 2.10: Voltage vs velocity data for all experiments as defined in Table 2.2. The model prediction can be compared to experimental data in PBS.

Figure 2.10 shows a plot with all 4 velocities representative of the 4 simulations, where the velocities shown are the average particle velocities from the simulations.

2.3.3 Further Validation of Models

Because the motion of DNA particles is dependent on the ionic concentration of the buffer solution, an additional set of experiments was conducted to isolate the effects of ionic concentration. The experiment was identical to the one described earlier with the following differences. The experiments were conducted at the following voltages: 1.5, 2.5, 3, 3.5, 4, and 5 V. The buffer solution used was TAE instead of PBS, with an ionic concentration of 0.04 M compared to 0.1514 M for PBS (roughly 3.8 times less concentrated). According to the data shown in Figure 2.11, the decomposition voltage for TAE/agarose is 1.8 V.

The data is shown in Figure 2.12, along with a least-squares line fit to the data at 1.8 V and above. Estimated measurement error bars for the velocity of DNA as a function of voltage are also represented in Figure 2.12. The error values are determined from the estimated displaced

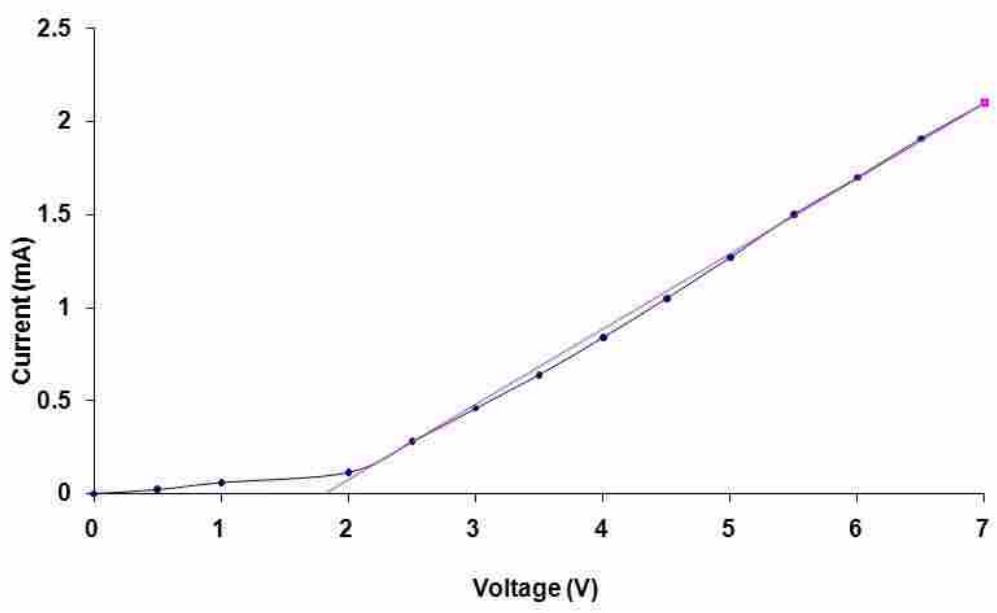

Figure 2.11: Effects of voltage on current in 30mg agarose/10ml TAE

measurement error value of ± 20 μm over the total time for each experiment. Figure 2.12 also shows the model's predictions for this case.

To further validate the model, another set of experiments was conducted to isolate the effects of DNA base pair size. The experiment used to obtain the results presented in Figure 2.12 was repeated except that DNA strands of 2000 base pair length were used instead of 4699 base pair strands. The results are reported in Figure 2.13, showing that the model correctly handles smaller DNA molecules.

Finally, the validated mathematical model presented above uses parallel plates close together where the electric field is uniform and perpendicular. The results are one dimensional DNA motion. To see how adaptable the mathematical model is to different electrodes configurations, the experiment shown in Figure 2.5 was conducted. The experiment ran for 60 minutes at 10 V. The buffer solution used was TAE with DNA strands of 2000 base pair.

Figure 2.14(a) shows the electrical field created by the electrodes. The field is represented by the randomly placed small arrows. The location of the electrodes and the DNA were selected to match the experimental set up found in Figure 2.14(b). The DNA has traveled away from the cathode and toward the anode as anticipated. Furthermore, the motion is multi-directional and tends to curve as it moves. A close look at the electrical field lines reveals that DNA motion follows

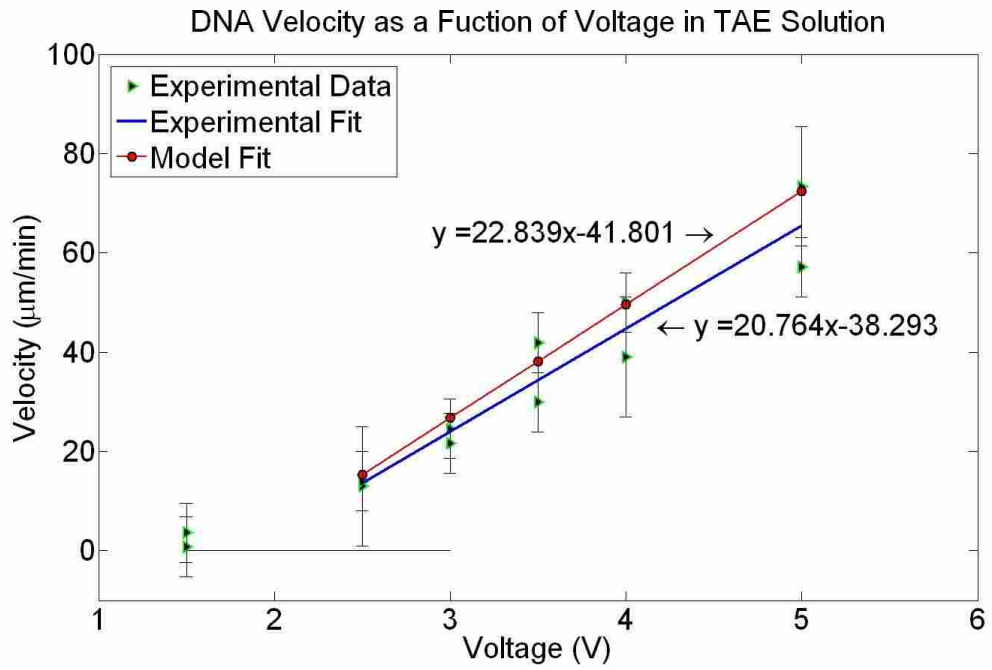

Figure 2.12: Modeling results compared to experimental data in TAE. The good agreement validates the model's predictions for varying solution molarity.

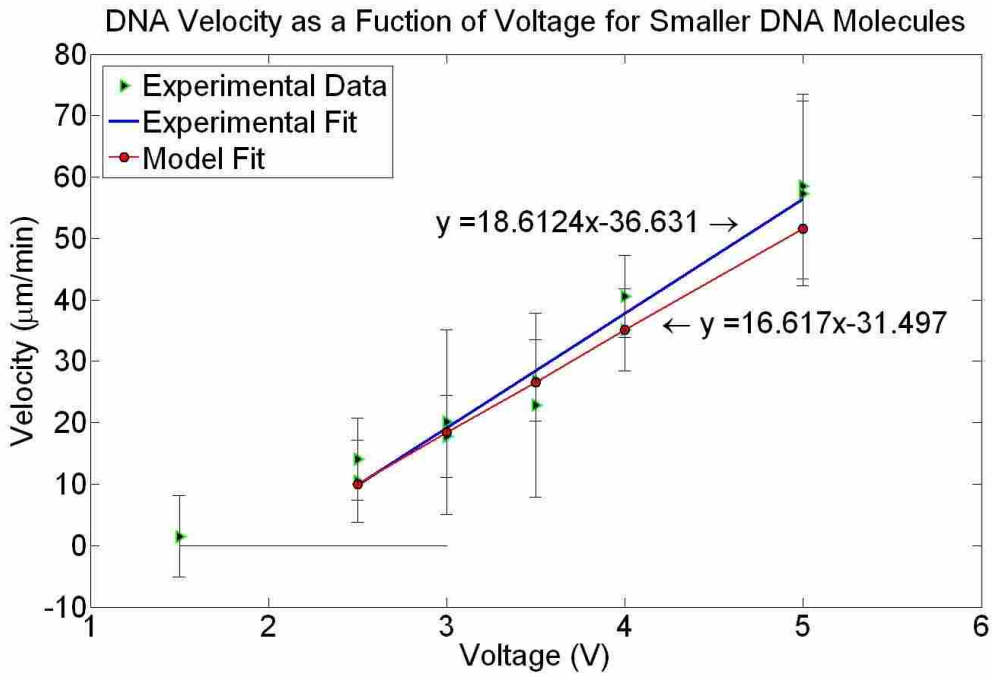

Figure 2.13: Modeling results compared to experimental data in TAE for smaller DNA molecules compared to Figure 2.12. The good agreement validates the model's predictions for varying DNA molecule size.

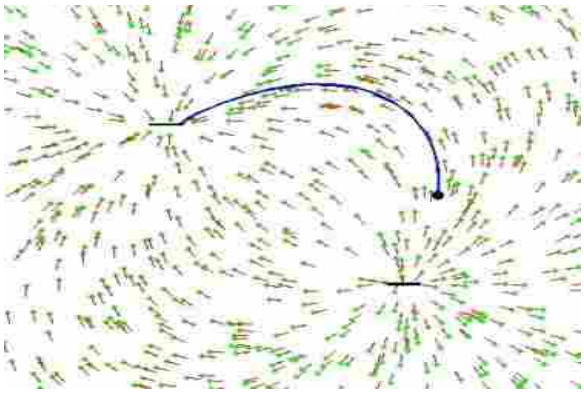

(a) Electric Field

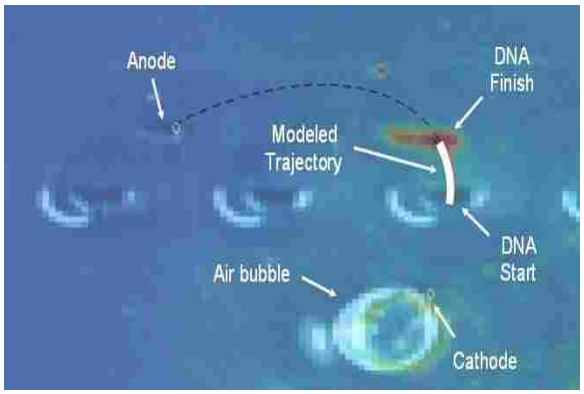

(b) Experimental Results

Figure 2.14: Comparison of DNA trajectory lines (Steel-Steel in 9 cm by 7.5 cm box - 60 minutes in 10 Volts)

Table 2.3: Two sample t-test for each experiment

Experiment	**Probability**
PBS	0.811
TAE 4699 bp	0.773
TAE 2000 bp	0.853

the electric field. The DNA trajectory is shown in both figures. The red trajectories in 2.14(b) leading to the final DNA position (experimental) represent the theoretical travel time of one hour.

2.4 Discussion

For each experiment, we wish to determine if there is a difference between the experimental and the modeled response (velocity). The null hypothesis is as follows: The experimental velocity is equal to the predicted velocity for the specified voltages. The results of a two sample t-test for each parallel plate experiment are tabulated in Table 2.3. In every case for each experiment, the test fails to reject the null hypothesis (P-value is greater than α, 5% or 0.05, the statistical level of significance) inferring that the velocities determined experimentally and those predicted by the computer model are not statistically different one from another. Therefore, for each case shown in Figures 2.10, 2.12, and 2.13, the measured velocity agrees within experimental uncertainty with the velocity predicted by the model. This shows the basic function of the model and it also

validates the use of the model for different ionic solutions (Figures 2.10, 2.12) and for different DNA molecule size (Figures 2.12, 2.13).

The results of the experiment with non-uniform field showed that the motion of DNA is multi-directional and follows the electric field (Figure 2.14). The experimental distance traversed is 0.6373 cm and the modeled distance is 0.6130 cm (4 % error). The direction of motion with respect to horizontal line for the experimental travelled distance is 100.54 degrees in comparison to 96.88 degrees for the modeled travelled distance (4 % error). Therefore, the model accurately predicts motion in a non-uniform electric field.

2.5 Conclusion

This chapter described the protocol for DNA motion using fabricated macroscale gel electrophoresis devices. Experiments to monitor and understand the displacement of DNA as a function of voltage, ionic concentration and DNA base pair size were conducted. The DNA was stained using EtBr, and microscope images (using UV light) were recorded at separate time intervals. MATLAB was used as the post processor to analyze pixel motion within each image saved. The results for each set of experiments were presented as a velocity vs. voltage plot (Figures 2.10, 2.12, 2.13). Figure 2.10 shows very similar shapes to the voltage vs current (V-I) plot shown in Figure 2.6. The average projected velocity decomposition voltage for Figure 2.10 is 2.82 V (compare to 2.94 V for the V-I curve in PBS). From these results, we can conclude that the velocity of DNA is correlated directly to current flow which in turn is controlled by the ionic solution and the voltage applied to the device.

The experimental voltage vs velocity curve was used to verify a mathematical model to predict the motion of DNA. The mathematical model is presented in detail to map the geometry and physical properties of the experimental set up. Simulations were analyzed in PBS media and TAE media. The simulated model provides results similar to the experimental results (Figure 2.10, 2.12, 2.13, 2.14). The good agreement between the model and the experiments validates the model's predictions. The model is verified and validated, including the prediction of accurate curved motion of DNA in the presence of a non-uniform electric field.

CHAPTER 3. EFFECTS OF DISSIMILAR ELECTRODE MATERIAL AND ELECTRODE POSITION ON DNA MOTION DURING ELECTROPHORESIS

3.1 Introduction

A mathematical model to predict the DNA motion during electrophoresis was previously created and validated with experimental results [56, 57]. While the results provided accurate prediction of DNA motion in different media (varying ionic concentration) and DNA size (base-pair length), the material used for the electrodes was a metal (steel).

In addition to our model, several previous models have been published to offer mathematical solutions of particle motion during electrophoresis [23–31, 58, 59]. However, none of these models integrate the electrode material as a parameter.

The intent of this chapter is to study the effects of dissimilar electrode materials on decomposition voltage, electrical field and DNA motion during electrophoresis. The experimental results are used to update the mathematical model to reflect the differences in material selection.

3.1.1 Motivation

We want to study the effects of dissimilar electrode materials on DNA motion using electrophoresis because our group at Brigham Young University has developed a MEMS-based lab-on-a-chip system (nanoinjector) for DNA injection. The experiments presented in this chapter will use a simplified macroscale physical representation of the nanoinjector shown in Figure 3.1. We want to understand and mathematically model the effects of dissimilar electrode materials on DNA motion.

Nanoinjection attracts and repels DNA to and from a solid silicon lance using electrophoresis [3, 33]. Electrophoresis is a term used when describing the movement of charged molecules in an ionic solution under the influence of an electric field. A prototype MEMS lance is shown in Figure 3.1. The lance acts as one electrode (silicon) for manipulating DNA using electrophoretic

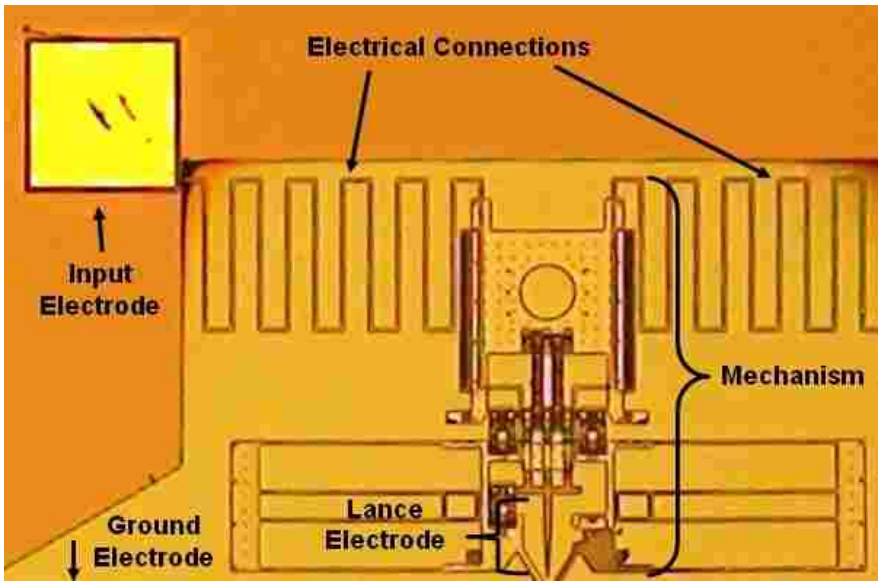

Figure 3.1: Image of the MEMS lance assembly (10x)

motion. The electrical connections represent the metal gold electrodes. For the experiments presented here, steel is used instead of gold for two reasons. First, around 3 volts, the gold layer deposited on a silicon wafer delaminates, making it hard to obtain reliable data. Second, the decomposition voltage of gold vs stainless steel in the buffered solution is similar so that both metals provide results that are approximately the same.

3.1.2 Decompostion Voltage

In an ionic (electrolytic) solution , the current flows as the ions present in the solution move, creating an electrical circuit (anions move towards the positive electrode while cations move toward the negative electrode) [57]. The current flow becomes significant above the decomposition voltage V_0 as shown in the sample I-V curve of Figure 3.2 [37]. The current above the decomposition voltage in an electrolyte is approximated as

$$I = \frac{(E - V_0)(\chi s)}{l} \tag{3.1}$$

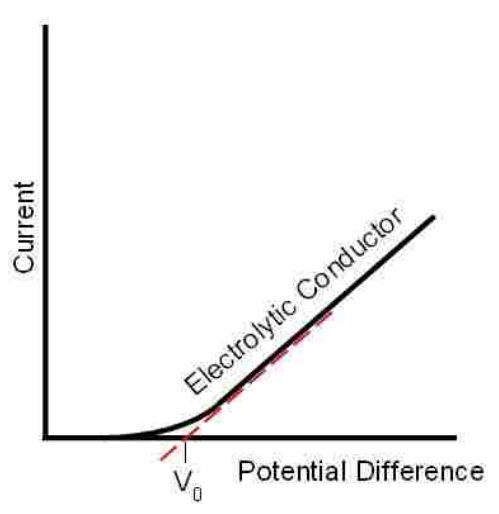

Figure 3.2: Ohm's law in electrolytes conductors (V_0 is the decomposition voltage)

where I is the current in amperes, E is the potential difference between the two electrodes in volts, s and l are the cross-sectional area and length of the conductor and χ is the specific conductance of the electrolyte.

3.2 Methods

3.2.1 Electrophoresis in Gel

The ionic solution (buffer solution) is necessary for electrophoresis since the electrical current allows for motion of charged particles [57]. The rate at which the molecules move depends on multiple factors (i.e. the charge carried by the molecule, its size and shape, the applied current and the resistance of the medium) [36, 60–62].

Figure 3.3 is a representation of the experimental set up used to study the effects of different materials in gel electrophoresis. The set up uses a 9 cm by 7.5 cm box where the gel is cooled. Three possible locations for electrodes are considered. In experiments using two electrodes, the anode and the top cathode are used. In experiments with three electrodes, the two cathodes are held at the same electrical potential. This setup models the nanoinjector, with one ground electrode and two other electrodes (the lance and the gold input pad) held at the same voltage.

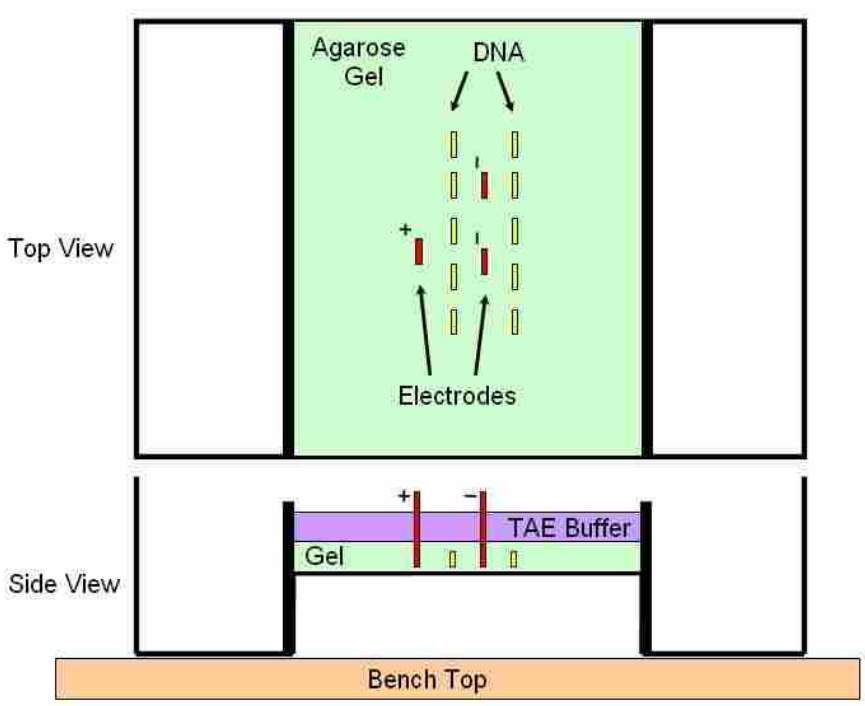

Figure 3.3: A schematic representation of experimental set up (dimensions are not to scale)

The protocol for the experiments will be described in detail later. After electrophoresis, the gel is imaged on a Bio-Rad Fluor-S MultiImager. This device is an imaging system capable of capturing high-resolution digital images from fluorescent samples. The gels are placed on the imaging surface of the MultiImager and the MultiImager door is closed. The gels are exposed to UV light for 20 seconds to produce an image of the stained DNA bands within the gel. The images produced are analyzed using Bio-Rad Quantity One computer software.

3.2.2 Mathematical Model Update

In previous work [32, 57], we showed mathematically how the decomposition voltage was included in the model to account for electrophoretic motion between two identical metal electrodes. The decomposition voltage value found in Equation 3.1 was subtracted from the value of the applied potential difference defined at the positive electrode. The negative electrode was assigned a value of 0 V. This approach worked well for cases with a single anode and cathode.

A revised approach is required to model a case like that shown in Figure 3.3, in which more than one electrode, possibly made from different materials, is held at the same potential.

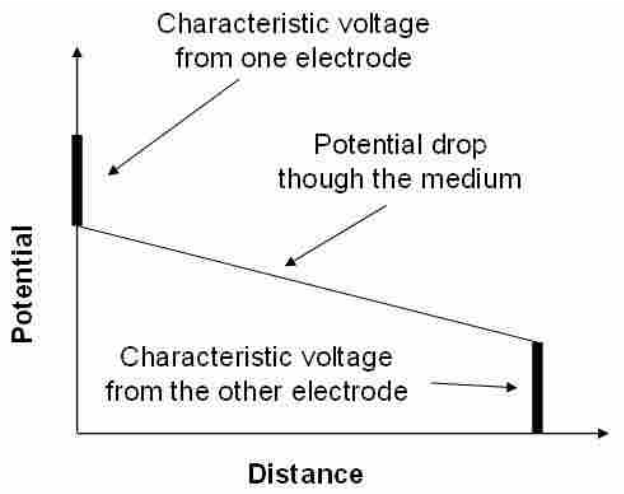

Figure 3.4: A schematic representation for the applied potential between two electrodes

Figure 3.4 is a representation of how the applied potential between electrodes is represented in the revised mathematical model. It can be divided into 3 regions. Region 1 and 3 represent the energy needed or the characteristic voltage for electrolysis for each electrode. For a different material, the characteristic voltage is different. Region 2 represents the potential drop through the medium. Because the value of the characteristic voltage is determined experimentally for different electrode materials, region 2 is obtained by subtracting the characteristic voltage of each electrode from the applied voltage. In effect, this approach considers each electrode to contribute a part of the total decomposition voltage, with the magnitude of the effect dependent on the electrode material.

3.3 Results

3.3.1 Experimental Decomposition Voltage

Equation 3.1 shows that significant motion is only possible when the voltage difference is above the decomposition voltage. As a result, experiments were conducted to determine the decomposition voltage under several conditions.

Steel and silicon are the materials used as electrodes. For each setup, two sets of voltage vs. current data were collected and the experimental decomposition voltage from both sets of data were averaged. Typical results for five electrode configurations are shown in Figure 3.5 with experimental decomposition voltage results summarized in Table 3.1. For each experiment, the

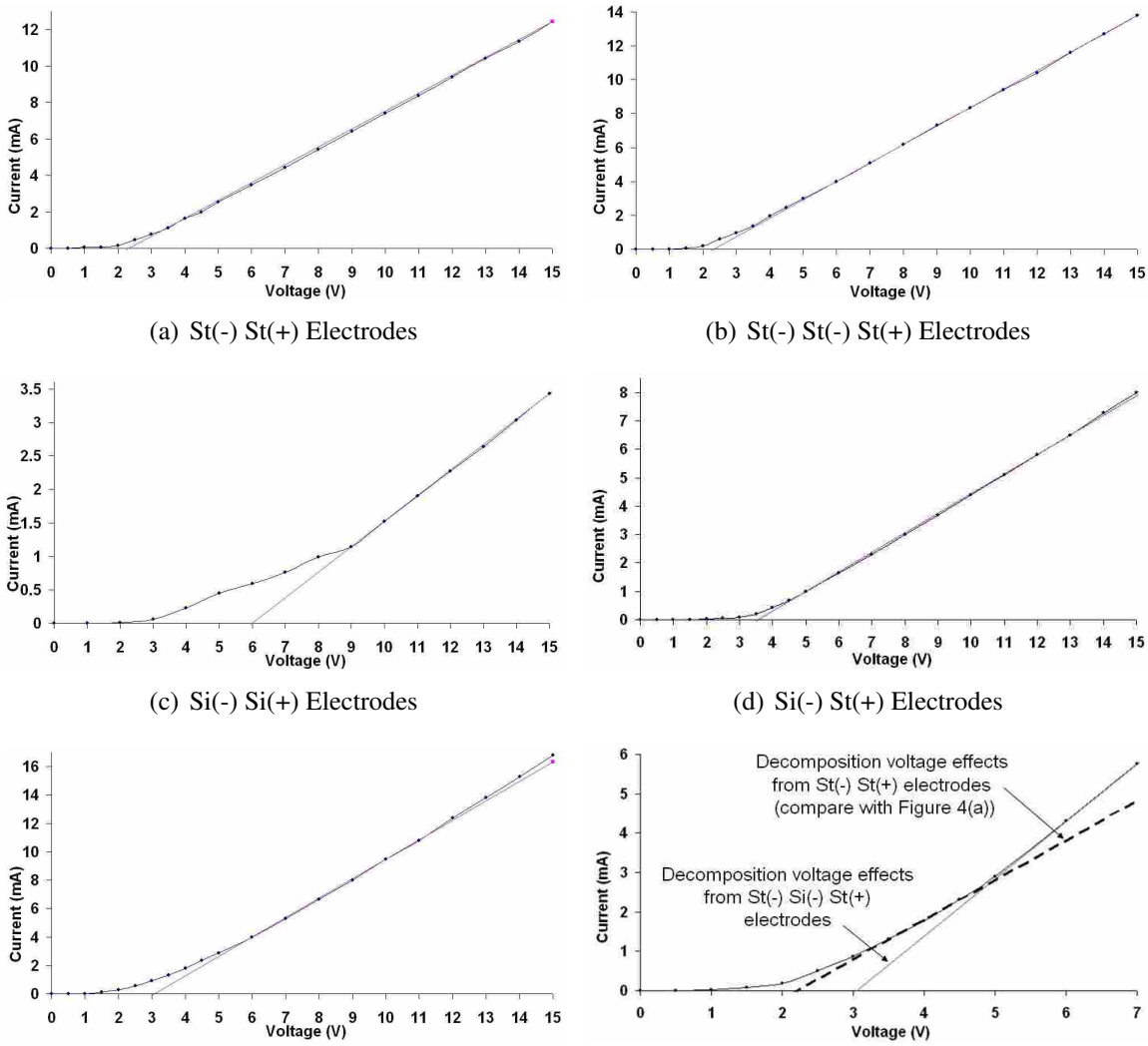

(a) St(-) St(+) Electrodes

(b) St(-) St(-) St(+) Electrodes

(c) Si(-) Si(+) Electrodes

(d) Si(-) St(+) Electrodes

(e) St(-) Si (-) St(+) Electrodes

(f) Close up of Figure 3.5(e)

Figure 3.5: Effects of voltage on current in 120mg agarose/40ml TAE

buffer solution consists of 40 ml of TAE (Tris-acetate-EDTA) mixed with 120 mg of agarose. Each electrode is 2.7 cm wide.

Note that the decomposition voltage for the St-St case (Figure 3.5(a)) is almost the same as that for the St-St-St case (Figure 3.5(b)). The material used in those two cases is the same, therefore we do not expect a significant difference in the decomposition voltage from the addition of one electrode. The voltage-current result from Figure 3.5(c) (Si-Si electrodes) shows the most irregularities. Silicon is a semiconductor susceptible to oxidation (creating glass) and the waviness pattern in the graph represents the electrochemical oxidation at the anode (impeding current flow).

Table 3.1: Summary of decomposition voltages. St represents a steel electrode and Si is a silicon electrode. (-) represents the cathode and (+) the anode.

Figure	Electrodes	Decomposition Voltage (V)
3.5(a)	St(-) St(+)	2.28
3.5(b)	St(-) St(-) St(+)	2.33
3.5(c)	Si(-) Si(+)	6.08
3.5(d)	Si(-) St(+)	3.53
3.5(e)	St(-) Si(-) St(+)	3.06

To avoid oxidation on the silicon for this study, silicon is used as the cathode in all other experiments with silicon. Figure 3.5(e) shows the current flow as a function of voltage for a St(-) Si(-) St(+) electrodes setup. The graph is representative of a typical electrolytic conductor. The decomposition voltage is reported to be 3.06 V. A close up of the graph (Figure 3.5(f)) shows that the silicon electrode does not contribute to the decomposition voltage until it reaches approximately 5 V. The linear dotted line estimates a decomposition voltage of 2.22 V, comparable to 2.28 V for Figure 3.5(a) (no silicon). Above 5 volts, the current flow becomes linear again and the effect of the silicon electrode becomes visible (increasing the decomposition voltage shown in Figure 3.5(e) and Table 3.1).

3.3.2 Characteristic Voltage for each Material

The characteristic voltage for each material used in the mathematical model (St and Si) is represented by the bold vertical drop (region 1 or 3) at each extremity on Figure 3.4. Based on the test results shown in Figure 3.5 and Table 3.1, its value for each material is defined as

$$V_{St} = \frac{V_{0,St(-)St(+)}}{2} = \frac{2.28}{2} = 1.14V \tag{3.2}$$

$$V_{Si} = V_{0,Si(-)St(+)} - V_{St} = 3.53 - 1.14 = 2.39V \tag{3.3}$$

From Table 3.1, 2.28 V is the value of the decomposition voltage for St(-) St(+) and 3.53 V for Si(-) St(+) respectively. The characteristic voltage drop for a steel electrode is calculated by halving the decomposition voltage for the St(-) St(+) case. Because of the irregularities of the

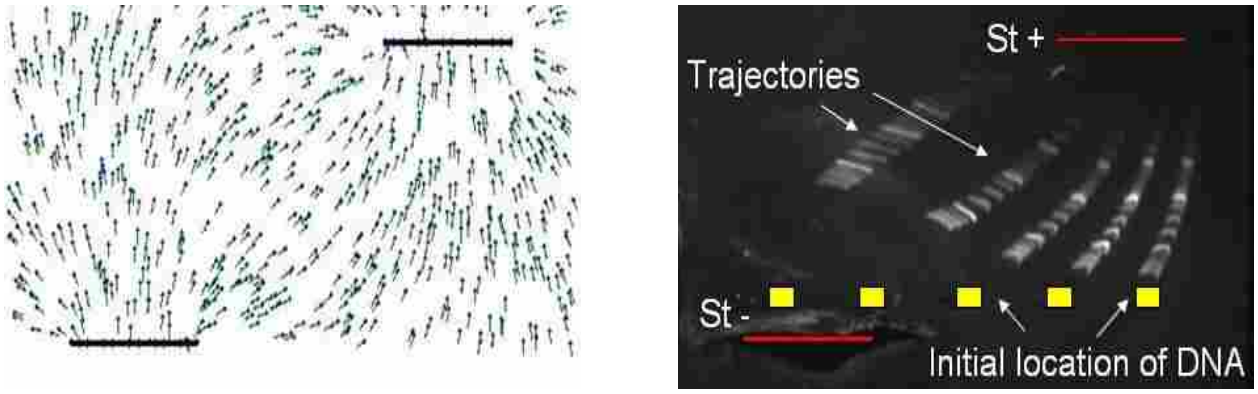

(a) Electric Field (b) Experimental Results

Figure 3.6: DNA ladder (St(-) St(+) in 9 cm by 7.5 cm box - 40 minutes at 60 Volts)

Si(-) Si(+) decomposition Voltage, V_{Si} was determined by subtracting the characteristic voltage for steel electrodes from the decomposition voltage for the Si(-) St(+) case. These two characteristic voltages were used for all subsequent modeling in this chapter.

3.3.3 DNA Motion Experiments

DNA Ladder Experiment

A DNA ladder is a solution of DNA molecules of different length and is used as a reference to estimate the size of unknown DNA molecules. The DNA molecules pass through the gel matrix at different rates forming clusters of DNA strands of similar lengths through the volume of the gel. The clusters provide a physical trace where the DNA has traveled. Using this approach, large curved-field motion of DNA particles during electrophoresis is observed. Another method which may be used for DNA detection is presented in [63]. Figure 3.6 shows results for an experiment at 60 Volts for 40 minutes in a 7.5 cm by 9 cm box. The location of the electrodes are graphically represented by two rectangles labeled St+ and St-. The initial location of the DNA and the trajectories are also specified. The electric field plot is added to show that the motion of DNA follows the electric field direction.

Further experiments to measure and quantify displacements are presented. Each experimental setup in Figure 3.5 and Table 3.1 was used to study DNA motion in the resulting electric field. DNA motion was measured in two identical replicates for each electrode configuration. The

gels were prepared as follow: 120mg of agarose in 40ml of TAE. Before the gels cooled, 0.4μl of Ethidium Bromide was added. Ethidium bromide (EtBr) is a fluorescent dye which intercalates between the stacked bases of DNA. EtBr is commonly used to stain double-stranded DNA separated in agarose gels. Grooves were formed where 3 μl of DNA (33 ng/μl - 2000 basepair) would be added to each groove.

St(-) St(+) Electrodes

The validated mathematical model presented in [57] used parallel plates close together where the electric field is uniform and perpendicular. The results showed one dimensional DNA motion. To see how adaptable the mathematical model is to different electrode configurations, the following experiment was conducted. Two thin steel electrodes were placed at an offset diagonal to each other. DNA was placed in grooves and 10 volts was applied for 60 minutes. The results are shown in Figure 3.7(b). The DNA has traveled away from the cathode and toward the anode as anticipated. Furthermore, the motion is multi-directional and tends to curve as it moves. A close look at the electrical field lines reveals that DNA motion follows the electric field.

Figure 3.7(a) shows the electrical field created by the electrodes, as simulated by the model [64–66]. The field is represented by the randomly placed small arrows. The location of the electrodes and the DNA were selected to match the experimental conditions found in Figure 3.7. Only the DNA between the plates are modeled and the trajectories are shown in both figures. The red trajectories in 3.7(b) leading to the final DNA position (experimental) represent the theoretical travel time of one hour. The results closely follow the prediction based on the model.

St(-) St(-) St(+) Electrodes

With the model shown to characterize the motion of DNA in the presence of an electrical field using two electrodes, three electrodes were studied.

The experiment setup and results shown in Figure 3.8 was conducted at 10 Volts for 120 minutes in a 15.8 cm by 14 cm box. The location of the electrodes are represented by the small white circles. We used a larger gel box to minimize the effects of physical boundaries on current

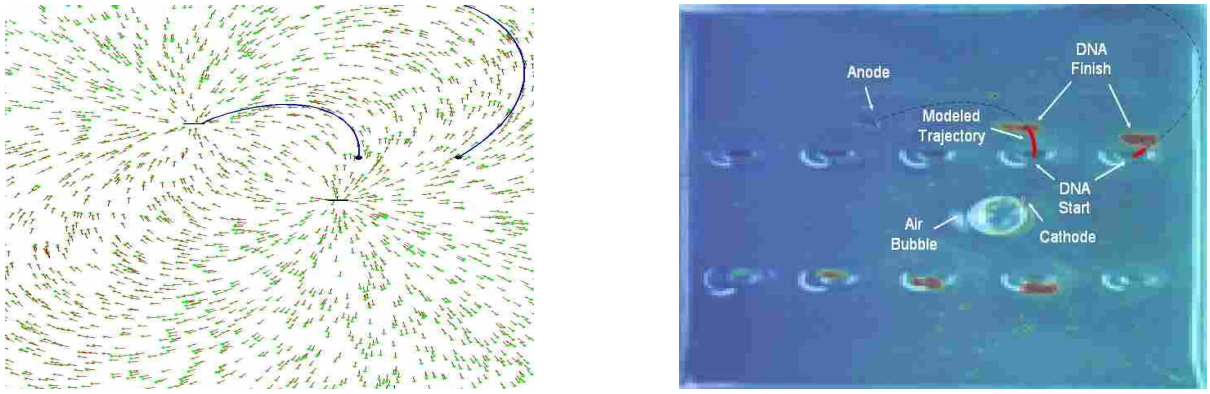

(a) Electric Field

(b) Experimental Results

Figure 3.7: Comparison of DNA trajectory lines (St(-) St(+) in 9 cm by 7.5 cm box - 60 minutes at 10 Volts)

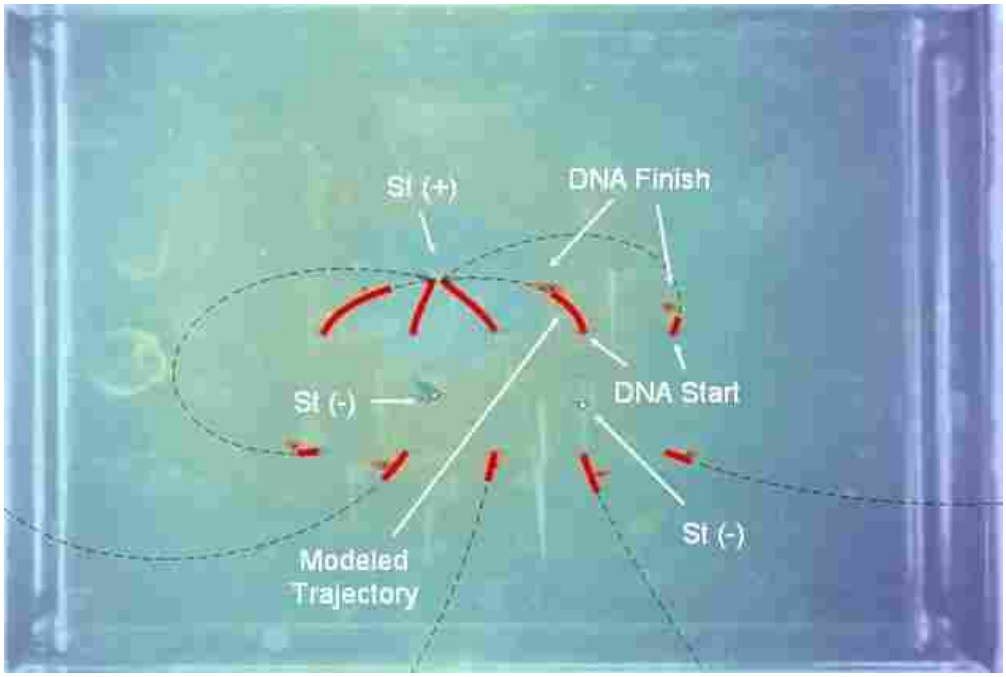

Figure 3.8: St(-) St(-) St(+) electrodes in a 15.8 cm by 14 cm box - 120 minutes at 10 Volts

and fluid flow (walls are not so close to the DNA and the electrodes), allowing direct comparison and validation of the model for three electrodes.

Table 3.2: Traveled distance of DNA for St(-) Si(-) St(+), Si(-) St(-) St(+) and St(-) St(-) St(+) electrodes

St(-) Si(-) St(+)	**Modeled (cm)**	**Experimental (cm)**	**Error (%)**
10 V for 60 min	0.38	0.44	13
10 V for 60 min	0.48	0.49	2
10 V for 120 min	1.01	1.05	4
St(-) St(-) St(+)	**Modeled (cm)**	**Experimental (cm)**	**Error (%)**
10 V for 60 min	0.39	0.45	13
10 V for 60 min	0.26	0.31	16
10 V for 120 min	0.82	0.93	12
Si(-) St(-) St(+)	**Modeled (cm)**	**Experimental (cm)**	**Error (%)**
5 V for 120 min	0.19	0.21	10
5 V for 120 min	0.17	0.21	19
St(-) St(-) St(+)	**Modeled (cm)**	**Experimental (cm)**	**Error (%)**
5 V for 120 min	0.40	0.36	11
5 V for 120 min	0.48	0.40	20

St(-) Si(-) St(+) and Si(-) St(-) St(+) Electrodes

The proposed hypothesis is that utilization of a silicon electrode instead of a steel electrode affects the motion of DNA. We also propose that the mathematical model can predict a difference in the motion using dissimilar electrode material. To test our hypothesis, we conducted the set of experiments (outlined in Table 3.2) in a 9 cm by 7.5 cm gel box. Figure 3.9 shows the position and type of electrode material used. For St(-) Si(-) St(+), the silicon electrode replaces the bottom left steel electrode. For Si(-) St(-) St(+), the silicon electrode replaces the bottom right steel electrode (see Figure 3.9(b)).

For each St(-) Si(-) St(+) experiment, a parallel experiment was conducted under identical conditions using St(-) St(-) St(+) electrodes. A comparison of the trajectories between modeled and experimental will reveal whether or not the material of the electrodes has a significant effect on DNA motion. Quantitative results for a DNA trajectory in each experiment are presented in Table 3.2 and some results are shown in Figure 3.9.

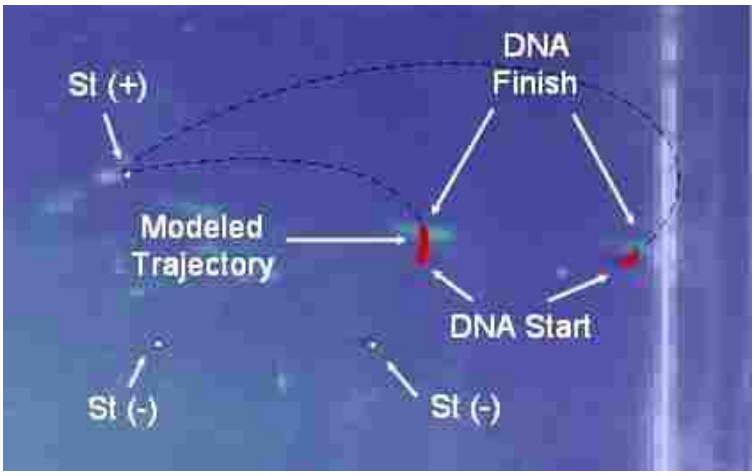

(a) St(-) St(-) St(+) in 9 cm by 7.5 cm box

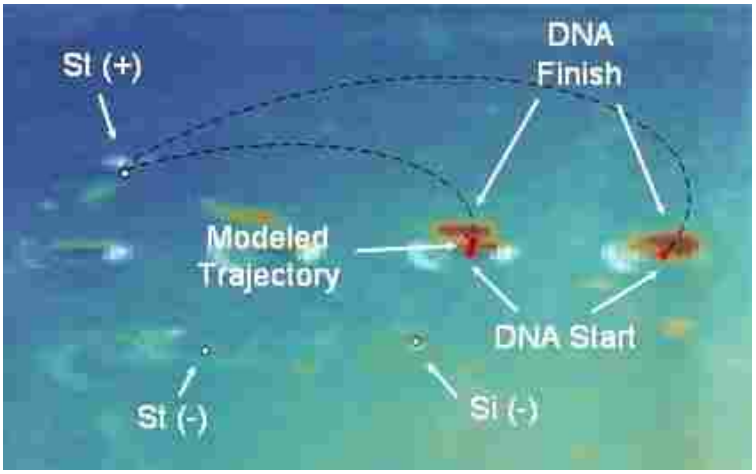

(b) Si(-) St(-) St(+) in 9 cm by 7.5 cm box

Figure 3.9: Comparison of DNA trajectory lines - 120 minutes at 5 Volts

3.4 Discussion

In the mathematical model, the DNA trajectories are calculated using a numerical integration approach within MATLAB (a technical computing software). Because the trajectories are time dependent, it is possible to obtain a travel distance over the time used in the experiments. The modeled distance can then be compared to the experimental image. Using the known width and the height values of the gel box and the pixel count per axis of the experimental image, a direct comparison between pixel size and pixel location (distance measurements) can be established for each experimental result. Both mathematical and experimental results for one experiment can be

Table 3.3: Comparison of modeled traveled distance of DNA for Si(-) St(-) St(+) and St(-) St(-) St(+) at 5 V

Si(-) St(-) St(+)	**Modeled (cm)**	**Modeled as St(-) St(-) St(+) (cm)**
5 V for 120 min	0.19	0.32
5 V for 120 min	0.17	0.36
St(-) St(-) St(+)	**Modeled (cm)**	**Modeled as Si(-) St(-) St(+) (cm)**
5 V for 120 min	0.40	0.19
5 V for 120 min	0.48	0.24

superimposed resulting in a graphical solution such as Figure 3.8. Quantitative results can be obtained for both mathematical and experimental results. Table 3.2 shows the traveled distance of one trajectory for each experiment. However, because of user uncertainty errors of $\pm 20\%$ (experiments prepared by user), a direct comparison between Silicon and Steel experiment does not lead to reliable results.

The error column found in Table 3.2 tells of the percent difference between the calculated and the measured DNA motion. For St(-) Si(-) St(+) and St(-) St(-) St(+) at 10 V, the average displacement in the presence of a silicon electrode is similar to the displacements with the all steel electrodes. According to Table 3.1, 10 V is significantly greater than the decomposition voltage for St(-) St(-) St(+) and St(-) Si(-) St(+) masking the small effects of the silicon electrode. The applied voltage was reduced to 5 V and the placement of the silicon electrode was changed (see Figure 3.9(b)). The percent error between the modeled and the experimental results for each experiment is within 20 % and the traveled distance of the steel electrode is twice that of silicon, showing the effects that electrode material can have on DNA motion.

Further analysis was conducted for each of the 5 V experiments to compare the prediction between materials using the model. For the Si(-) St(-) St(+) modeled simulations, we replaced the silicon electrode with a steel electrode leaving all other parameters untouched (see Table 3.3). The distance travelled (using the model) jumped from 0.19 cm to 0.32 cm and 0.17 cm to 0.36 cm. Similarly when the St(-) St(-) St(+) was substituted by Si(-) St(-) St(+) in the model, 0.40 cm of traveled distance reduced to 0.19 cm and 0.48 cm reduced to 0.24 cm (see Table 3.2 for modeled trajectories). The modeled results validate the hypothesis that electrode material affects the motion of DNA (distance travelled for steel is about twice that of silicon).

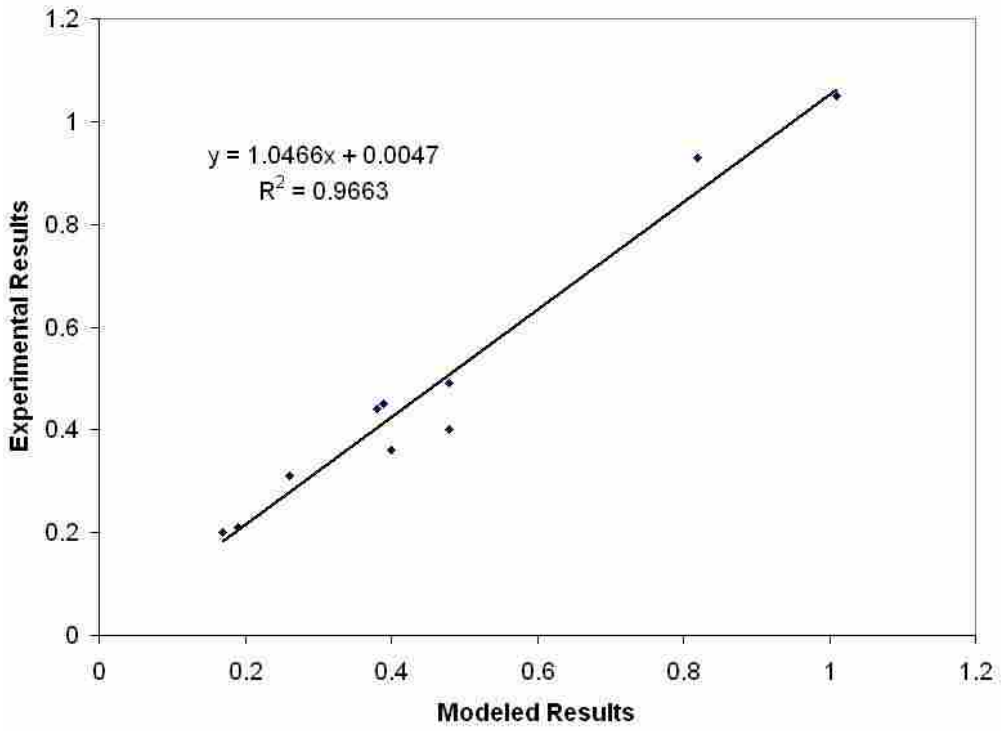

Figure 3.10: Linear dependence between modeled and experimental results from Table 3.2

A final analysis shows that the modeled results and the experimental results are linearly dependent (Pearson Correlation value R of 0.9830). See Figure 3.10 for details. This result further confirms the validity of the model.

3.5 Conclusion

This chapter studies the effects of different electrode material on decomposition voltage, electrical field and DNA motion. Experimental results are used to update the mathematical model to reflect the differences in material. We also showed that our model predicts large curved-field motion of charged particles during electrophoresis (Figure 3.7).

The validated mathematical model presented in [57] used parallel plates close together where the electric field is uniform and perpendicular. To see how adaptable the mathematical model is to different electrode configurations, two thin steel electrodes were placed at an offset diagonal of each other. The results showed that the motion of DNA is multi-directional and follows the electric field (Figure 3.7).

A simplified electrode set up for the nanoinjector was studied (three electrodes representing two electrical connections and the tip of the lance). We conducted an experiment using 3 steel electrodes in a large gel box (15.8 cm by 14 cm) where the walls were not so close to the DNA and the electrodes. This minimized the boundary effects on the experimental trajectories, validating the model for three steel electrodes. The model can be used to accurately predict motion of DNA under 2 or 3 electrodes (independent of spatial positioning) made of steel.

Because the nanoinjection lance is fabricated from silicon, we studied material effect on DNA motion. To test the hypothesis that electrode material (Si and St) does affect the motion of particles, we conducted a set of experiments at 10 V and at 5 V (Table 3.2). The results show that electrode material does have a significant effect on DNA motion, especially when the applied voltage is near the decomposition voltage for the system.

We also showed excellent correlation between experimental results and simulations, indicating the power of the model in predicting DNA motion. The next step is to use the model to study and improve the nanoinjection process.

CHAPTER 4. STUDY OF DESIGN PARAMETERS AFFECTING THE MOTION OF DNA FOR NANOINJECTION

4.1 Introduction

Our research group has developed a micro-electro-mechanical system (MEMS) based lab-on-a-chip system for DNA injection. A prototype MEMS lance is shown in Figure 4.1. Our innovative approach, called nanoinjection, differs from traditional microinjection which uses a pump to channel the injected substance though a hollow microneedle into the cell [1, 2, 5]. In comparison, nanoinjection uses electrical forces to attract DNA or other charged macromolecules to a solid lance and repels the attracted DNA into the cell. In this way, the entire injection process can be performed on a chip without the requirement for macroscale pumps. In addition, the method may be automated to decrease the time and cost required for injection.

We have previously presented a model describing the repulsion of DNA into a cell and we have validated the model by experiments [32, 56, 57]. Here we apply the model to both attraction and repulsion and we present a study of the effects of modeled parameters on DNA motion. Our data provides a better understanding of the nanoinjection process. The results will be used to improve the nanoinjection design and process.

4.2 Background

4.2.1 The Nanoinjector and Electrophoresis

The nanoinjector consists of a solid protruding element (the 'lance') that is raised out of the plane of fabrication, is electrically charged to attract DNA, pierces the membrane of a cell, and repulses the DNA inside the cell. Figure 4.2 shows a diagram of the device within a culture dish, piercing and repelling DNA inside of a cell. Using the nanoinjector, we are injecting mouse

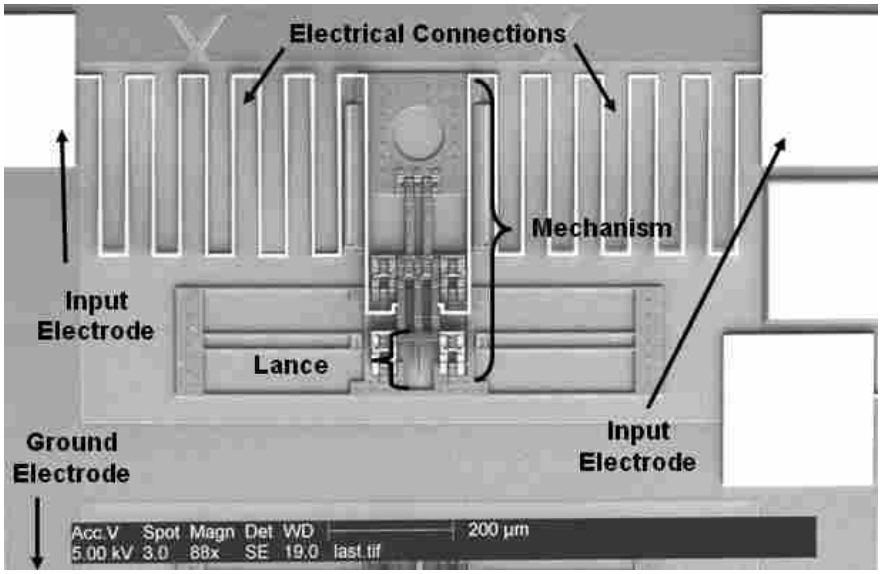

Figure 4.1: Scanning electron micrograph of the MEMS lance assembly

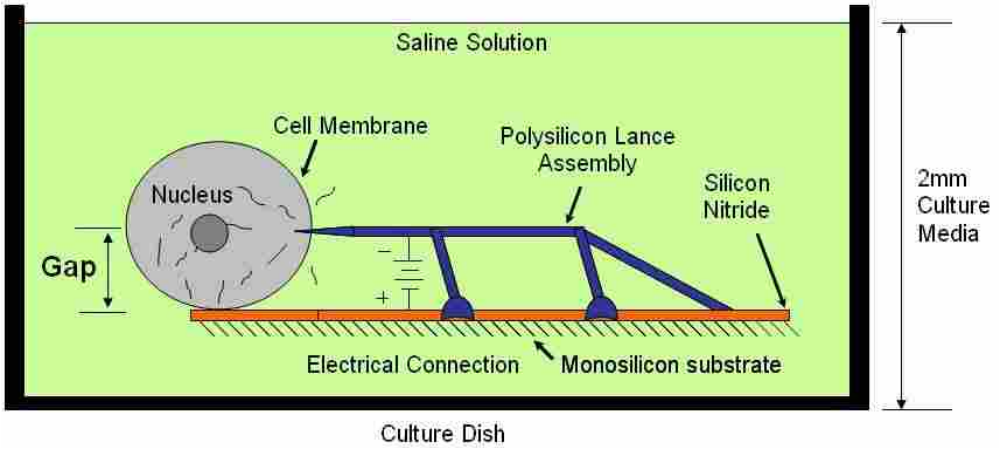

Figure 4.2: Diagram of nanoinjector with the gap parameter identified

egg cells to demonstrate the method for transgenic mice production. This chapter studies such injections using a model study to predict the importance of design and injection parameters.

DNA can be manipulated electrically because it is a charged particle. The phosphate backbone of the DNA has a net charge of one electron per phosphate, giving a total of two electrons per base pair [9]. Moving particles using the electric field generated by electric charges is called electrophoresis. This method has been used for transportation, separation and characterization of

bioparticles by researchers [13–22, 34, 35]. In addition, our lab has shown attraction of DNA to the MEMS lance using electrophoresis [33].

4.2.2 Mathematical Model

Previous work [32,57] describes the model proposed to determine the motion of DNA using nanoinjection (compare with models found in [23–31], which treat only uniform electric fields). Our model has two main parts. They are described below.

First, the model predicts the electric behavior around the lance due to the potential difference between the lance and the ground electrode. No exact closed-form solution is available for the complex geometry; therefore, a numerical solution was developed. The Boundary Element Method (BEM) is used to calculate the charge density on each electrode. The resulting charge distribution collected on the surfaces of the conductors is then used to calculate the electric field.

Second, the model predicts the macromolecular motion of DNA due to the electric field created from the charges on the surfaces of the conductors. An applied electric force, a viscous resistive force, and an electrophoretic retardation force [52] are considered to act on a DNA particle. The sum of the forces defines the acceleration of the particle. The position and velocity can then be determined from the acceleration. The model has been verified and validated against experimental results [32]. In addition, the model accurately predicts large curved-field motion of charged particles in the presence of a non-uniform electric field created by similar or dissimilar electrodes [32].

4.3 Methods

4.3.1 Modeling Attraction and Repulsion

To better understand the entire nanoinjection process, we study the attraction and repulsion of DNA under changes in design and operating parameters. The modeling differences between attractive and repulsive modelling are:

- Mesh refinement of lance (Fine for attraction, coarser for repulsion)
- Potential on lance (Positive for attraction, negative for repulsion)

Table 4.1: List of parameters

Parameters	Reference Simulation	Comparison
Gap	47 μm	30 μm
Lance Direction	Away	Toward
Ground Electrode Location	Away	Under
Lance Tip Width	0.15 μm	1 μm
Lance Tip Half Angle	2.5 $^\circ$	5 $^\circ$
Lance Tip Height	1.5 μm	0.5 μm
Lance Orientation	Parallel	Perpendicular
Penetration Depth (% of lance)	75%	50%

- Initial position of DNA particles (Far from lance for attraction, near/on lance for repulsion)
- Physical constraints (Trajectory stops when DNA motion reaches the lance for attraction and cell wall for repulsion)

4.3.2 Parameters under Study

The model was used to explore the effects of changing parameters for nanoinjection. Each parameter is described below, and Table 4.1 lists the reference and changed values for comparison. The reference values correspond to the parameter values used in the nanoinjector hardware and experiments. The changed values represent a set of values different from the reference in order to compare the results. Each parameter was studied to determine its significance during nanoinjection by comparison to the reference simulation representing the experimental nanoinjection design and protocols. Simulations were performed to test each parameter by changing only that parameter's value while keeping all other parameters equal to the reference value. The effect of each change was measured by comparing the following with the reference simulation: the number of DNA molecules attracted to the lance, the placement of attracted molecules on the lance for repulsion into the cell, and the time required for attraction and repulsion.

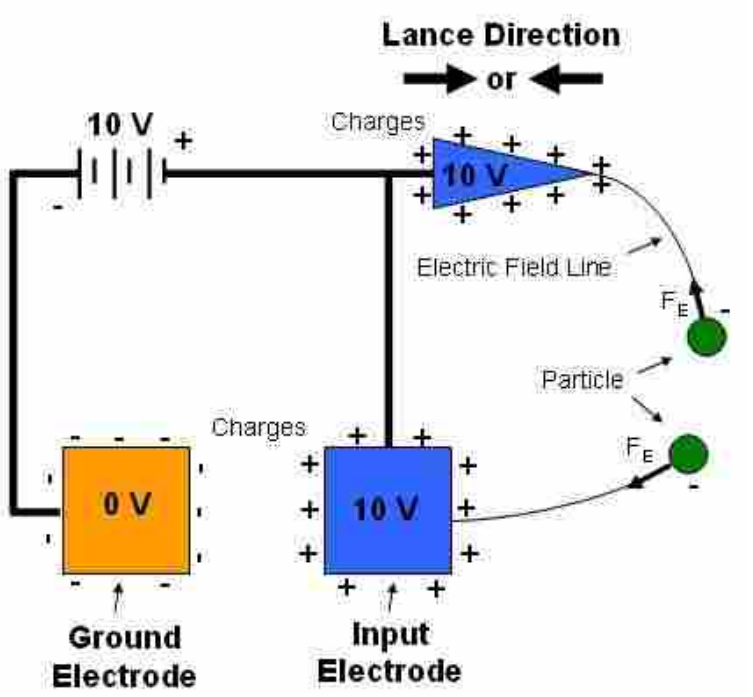

Figure 4.3: Lance direction (away) and ground electrode location (away) parameters

Gap, Lance Direction, and Ground Electrode Location

The gap between the substrate and the lance is mainly determined by the size of the cell that is to be injected. The gap parameter between the lance and the substrate electrode is defined in Figure 4.2. The nanoinjector is designed to pierce a cell along its line of symmetry (half the diameter of the cell). The gap values of 47 μm and 30 μm presented in Table 4.1 would be used to inject cells (on average) of diameter 94 μm and 60 μm respectively.

The lance direction parameter is defined by having the lance pointing either away or toward the ground electrode (see Figure 4.3). We have fabricated lances in both directions; this parameter allows us to test whether the lance direction affects injections.

The ground electrode location parameter represents whether the ground electrode is directly placed under the lance or away from the lance (see Figure 4.3). The current design places the ground electrode away from the lance, but the design would be more compact if the ground electrode were placed under the lance. This parameter allows this alternate design to be tested.

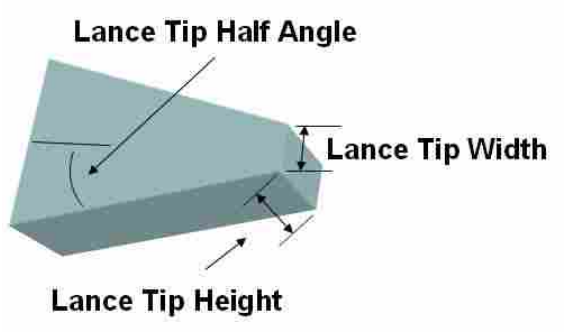

Figure 4.4: Lance tip width, lance tip half angle, and lance tip height parameters

Even though the input electrode is not a parameter under study, it represents the bond pad used to place voltage on the lance (see Figures 4.1 and 4.3). The input electrode is included in the mathematical model to understand and measure its effect during nanoinjection.

Lance Tip Width, Lance Tip Half Angle, and Lance Tip Height

The minimum lance tip width is constrained by the fabrication process limitations. 150 nanometer is the smallest tip width at which the lance can be fabricated using the current process [8] and is the value used as the reference. Similarly, the maximum lance tip width is constrained by the size of the cell and the damage inflicted on the cell when punctured by a rectangular tip. The comparison value for this study is 1 μm.

Figure 4.4 is a schematic representation of the lance where the lance tip width, lance tip half angle, and lance tip height parameters are defined. The lance tip half angle is described as half of the full angle made by the sides of the lance. Increasing the tip half angle increases the base width of the lance. The reference value is 2.5 °, which will be compared to a lance tip half angle of 5 °.

The tip height parameter allows the lance to be transformed from a wedge 1.5 μm thick (the reference) into a pyramidal tip (0.5 μm by 0.5 μm) for the comparison. A tapered height may reduce the trauma upon penetration of the lance into the cell, although the wedge-shape lance is easier to fabricate.

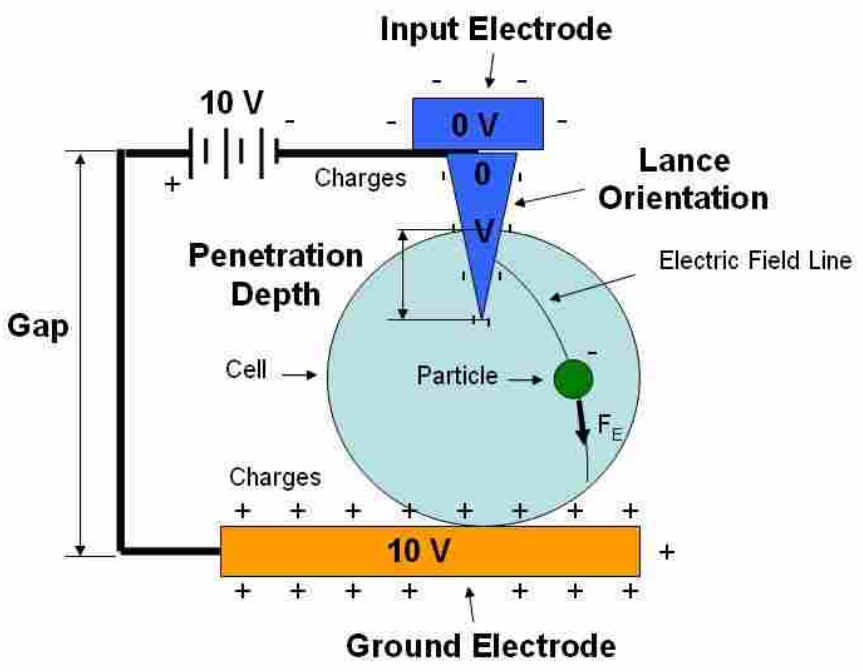

Figure 4.5: Lance orientation and penetration depth parameters

Lance Orientation and Penetration Depth

Another parameter of interest is the rotation of the lance relative to the substrate. The lance may be either parallel to the substrate (reference simulation and current design) or perpendicular to the substrate (comparison). Perpendicular lances have the benefit of being able to inject many cells simultaneously. They can be fabricated as an array of lances [67–69] used to deliver the same genetic material to a large number of cells at a time. Figure 4.5 shows one lance in the perpendicular orientation. In the perpendicular orientation, the input electrode is placed immediately above the lance to represent the lance's substrate. The ground electrode is placed beneath the cell.

Figure 4.5 also illustrates the penetration depth parameters. The depth of the lance inserted into the cell during injection is the final parameter of interest. It is only applicable during repulsion. In the reference simulation, the lance penetrates 75% of the cell's diameter. The comparison value is 50% of the diameter.

Table 4.2: Dimensions for the geometry of the lance, the substrate, and the input electrode (attraction and repulsion)

Dimensions	**Lance**	**Ground Electrode**	**Input Electrode**
Length x (μm)	124	240	250
Length y (μm)	11	240	250
Length z (μm)	1.5	0.5	0.5
Offset x (μm)	4086	0	3357
Offset y (μm)	1499	0	2105

Table 4.3: Other parameters for the simulation

Gap (μm)	47	Voltage (Volts)	10
Particles #	50	Charge (pC)	-3.2×10^{-5}
Mass (ng)	1.7×10^{-9}	Particle radius (μm)	0.0121
Basepair	1599	Viscosity (N·s/m^2)	6.924×10^{-4}

4.3.3 Attraction and Repulsion Simulation Parameters

A comparison study of design and operating parameters was conducted to investigate each parameter's effect on the efficiency of nanoinjection. The results presented here have been modeled using 50 particles. A solution can be obtained reasonably fast for 50 particles while maintaining a comfortable level of accuracy for describing the process and understanding the results. This is many times fewer than the expected number of particles actually used in nanoinjection (estimated in the thousands), but it provides a representative sample of DNA motion.

The current design of the lance is 1.5 μm thick and tapers at a 5 $^\circ$ angle from a minimal tip width of 150 nm to a maximum base width of 11 μm [33]. The MEMS nanoinjector is fabricated using the polyMUMPs fabrication technology, which provides two structural polysilicon layers and a gold layer [8].

Tables 4.2 and 4.3 list the parameters used for the attraction and repulsion model. Length x, length y and length z represent the dimensions for the lance, the ground electrode and the input electrode. Offset x and offset y represent the distances from the ground electrode to the lance and the input electrode (see Figure 4.6 to compare graphically). The lance is pointed away from the ground electrode for the reference simulations. The input electrode represents the bond pad

Table 4.4: DNA volume and out-of-bound constraints dimensions

DNA volume	**X**	**Y**	**Z**
Max (μm)	4831	1834	329.75
Min (μm)	4086	1174	12.75
Out-of-bound constraints	**X**	**Y**	**Z**
Max (μm)	6074	2605	800
Min (μm)	-250	-250	1.5

used to create an electrical connection to the lance. Because the bond pad is also an electrode, DNA particles will be attracted to it (as shown in Figure 4.6). For the attraction simulation, 50 DNA particles were randomly selected within a volume of dimensions described in Table 4.4. This volume is placed in front of the lance, where DNA is placed during our nanoinjection experiments. The out-of-bound constraints or limits due to the culture dish size are also defined in Table 4.4. The origin of the reference system is the bottom left corner of the substrate.

4.4 Results and Discussion

4.4.1 Study of Model Parameters

The simulations presented below are compared with the results of the reference simulations. The results for each simulation corresponding to the list of parameters found in Table 4.1 are compared with the results of the reference simulation shown in Figures 4.6 through 4.8. In each comparison simulation, all parameters except the one being studied are the same as the reference. A summary of the results are found in Table 4.5. Graphical results are helpful because we can visually track the motion of DNA particles during attraction and repulsion.

4.4.2 Reference Simulations

Graphical results for the reference attraction simulation are presented in Figures 4.6 and 4.7. Figure 4.6 shows that not all particles are attracted to the lance (40 out of 50). 10 out of 50 DNA particles were attracted to the input electrode. Figure 4.7 shows a close up of the location of the attracted DNA on the lance. The electric field is the greatest at the tip of the lance attracting a greater portion of the DNA. The first attracted particle displaced 14 μm in 1.1 ms (particle number

Table 4.5: Summary of results between parameters

Influence	Parameters	Attraction		Repulsion		Order
–	Reference	40/50	14 μm / 1.1 ms	36/40	17 μm / 1.9 ms	First
		DNA	916 μm / 17 s	DNA	47.1 μm / 13.4 ms	Last
Weak	Substrate / Lance Gap	40/50	31.5 μm / 5.5 ms	36/40	17.3 μm / 1.8 ms	First
		DNA	918 μm / 17 s	DNA	48.3 μm / 13.5 ms	Last
Weak	Lance Direction	40/50	14.4 μm / 1.2 ms	36/40	7.43 μm / 0.4 ms	First
		DNA	896 μm / 13.3 s	DNA	47 μm / 13.5 ms	Last
Strong	G. Electrode Placement	6/50	13.6 μm / 0.3 ms	5/6	24.4 μm / 1 ms	First
		DNA	398 μm / 0.87 s	DNA	46.9 μm / 4.5 ms	Last
Weak	Lance Tip Width	40/50	13.5 μm / 1 ms	37/40	14.2 μm / 1.3 ms	First
		DNA	927 μm / 17 s	DNA	46.5 μm / 13.1 ms	Last
Weak	Lance Tip Half Angle	41/50	15.1 μm / 1.3 ms	37/41	9.82 μm / 0.7 ms	First
		DNA	911 μm / 15.7 s	DNA	45.9 μm / 12.3 ms	Last
Weak	Lance Tip Height	40/50	13.7 μm / 1.1 ms	36/40	11 μm / 0.9 ms	First
		DNA	923 μm / 17 s	DNA	47.5 μm / 14.2 ms	Last
Strong	Lance Orientation	16/50	40.39 μm / 3.9 ms	–	–	First
		DNA	213.9 μm / 49.8 ms	–	–	Last
Strong	Penetration Depth	–	–	32/40	12.33 μm / 1.2 ms	First
		–	–	DNA	50.2 μm / 26.5 ms	Last

6). It is defined as the particle that traveled the fastest from its initial location to the lance. The last attracted particle displaced 916 μm in 17 s (particle number 10). It represents the particle with the slowest trajectory to have reached the lance.

To simulate the complete attraction/repulsion process, the final coordinates of the 40 attracted DNA particles are used as the initial position for the repulsion simulation. The lance penetrates 75% of the cell's diameter through its center, resulting in 36 out of the 40 attracted particles found within the cell. Figure 4.8 shows the repulsion results. The first repulsed particle displaced 17 μm in 1.9 ms (particle number 27). The last repulsed particle displaced 47.10 μm in 13.4 ms (particle number 8). Similar to the attraction the first and last repulsed particle correspond to the fastest and slowest particle to have been repelled from the lance.

The results from the reference simulation are the basis for the comparison study. Results presented in Table 4.5 for each simulation for all parameters are compared carefully to the results of the reference simulations. An influence factor is determined from the comparison. We propose

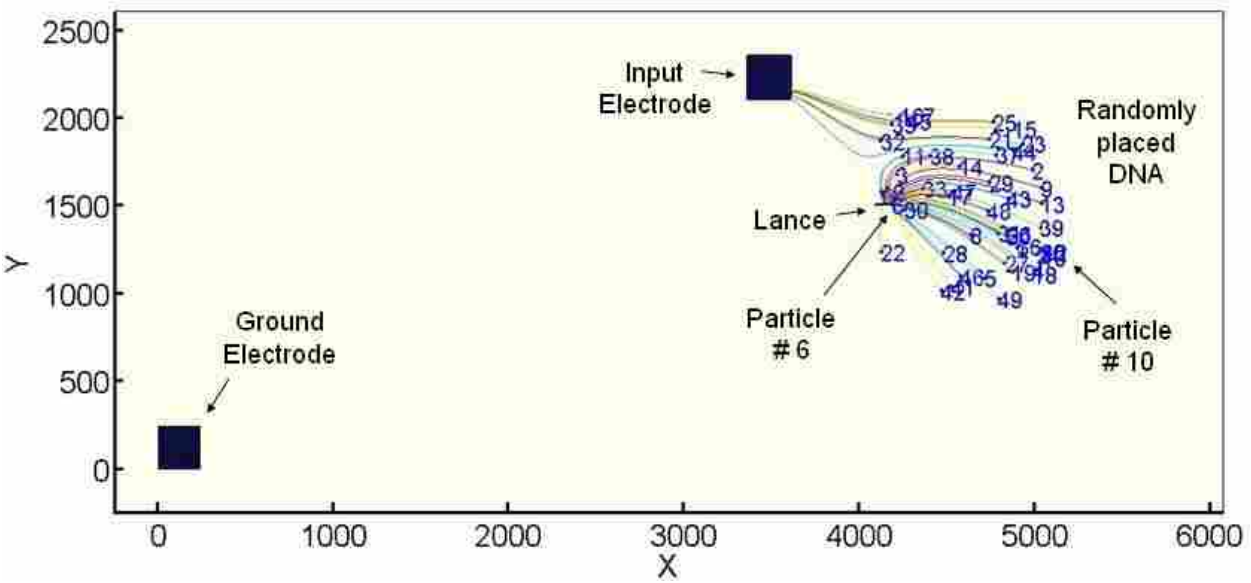

Figure 4.6: Top view of simulation of 50 DNA particles attracted to the lance and input electrode from random locations away from the lance (reference simulation)

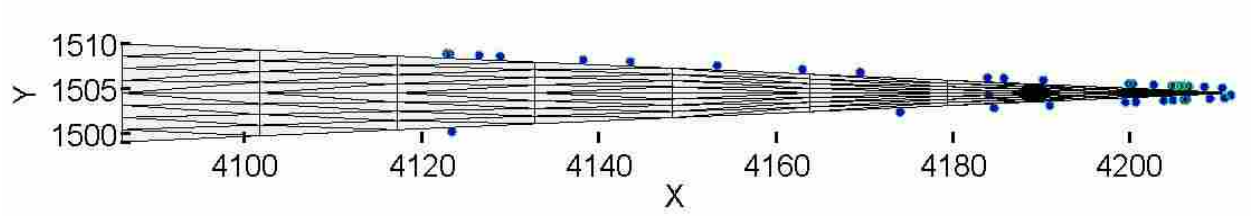

Figure 4.7: Location of attracted DNA particles - tip of the lance (reference simulation)

that a parameter has either a weak influence or a strong influence affecting nanoinjection. Because nanoinjection is a co-joint process between attraction and repulsion, the influence of a parameter is ranked by the overall number of DNA attracted and repelled during nanoinjection. A weak influence is the result of a small compared difference of the number of attracted and repelled DNA molecules between the reference and the comparison (less than 5% difference). A strong influence for an individual parameter results from a compared difference greater than 5%.

Gap

We compared the reference results, using a gap of 47 μm, to a simulation with a gap of 30 μm, representing a lance designed to inject cells with 60 μm in diameter. Every parameter

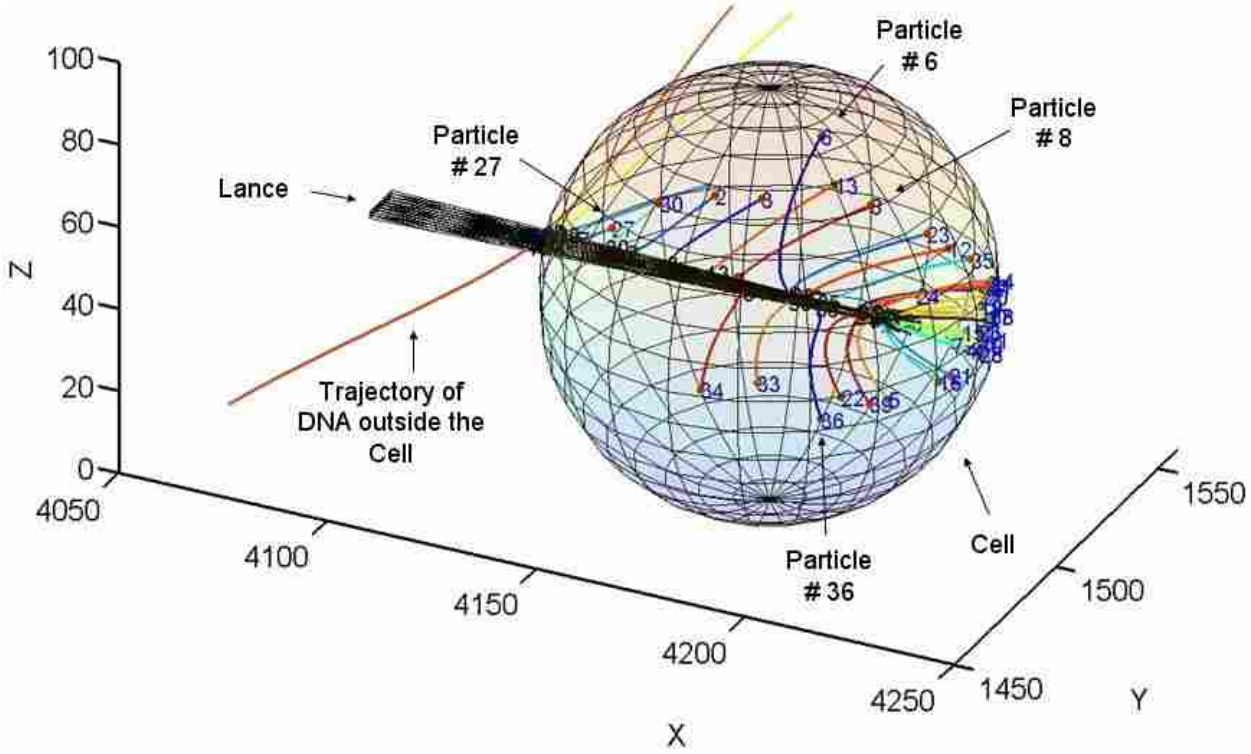

Figure 4.8: Simulation of 36 DNA particles repulsed within a cell (reference simulation)

including the initial location of the 50 DNA particles was identical. The first attracted particle travelled further and slower while all other measured results remained unchanged. Lowering the lance relative to the original DNA placement increases the distance between near-lance particles and the lance, explaining the increase in time and distance traveled for the first attracted particle. Overall, when the lance is lowered and the substrate and input electrodes remain unchanged, the influence of the gap parameter is weak (0% difference in the overall number of attracted and repelled DNA).

Lance Direction

The lance direction is the parameter that allows the lance and the input electrode to be reflected about the x-axis such that the lance direction points toward the ground electrode. To adjust for the change in the lance direction, the initial placement of the DNA is reflected and translated. The number of attracted and repelled particles is identical to the reference simulation. The direction of the lance with respect to the substrate shows a noticeable time difference and distanced traveled

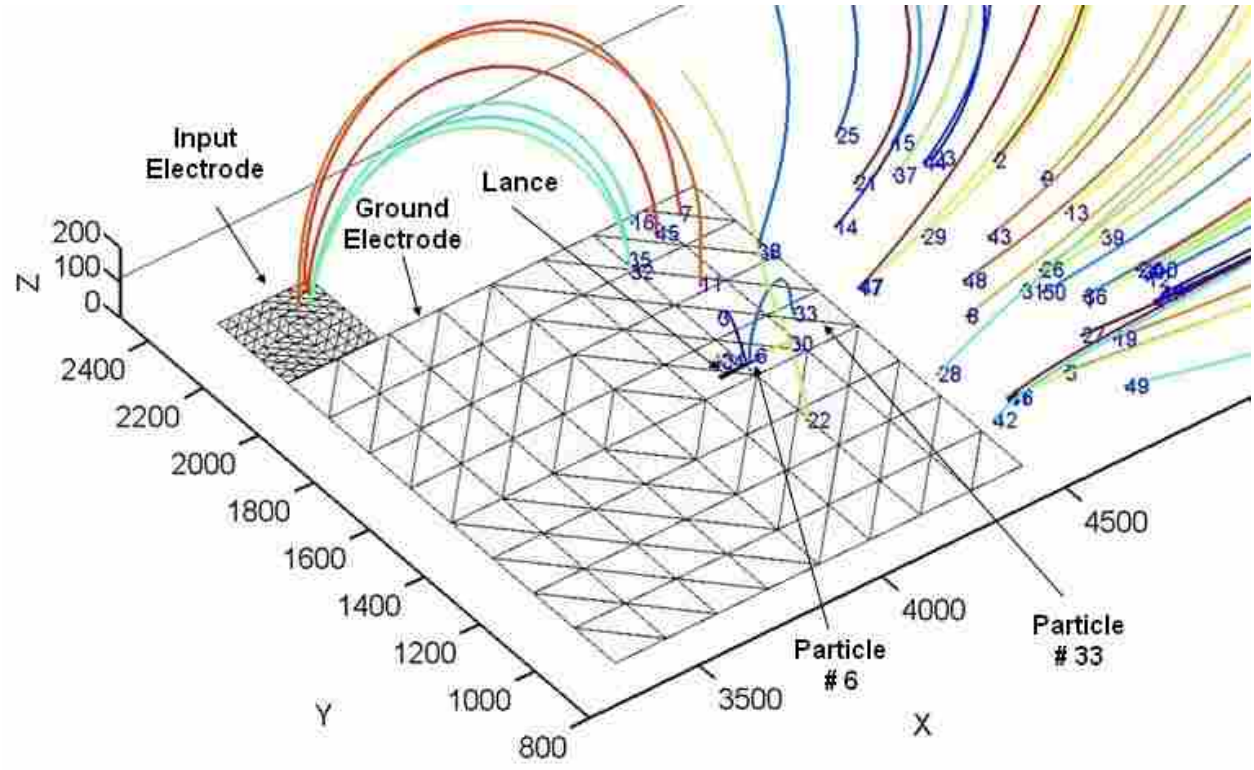

Figure 4.9: 6 out of 50 simulated DNA particles attracted. Large substrate underneath the lance with input electrode (ground electrode placement simulation)

for the last attracted and the first repelled particle. When the lance points in the direction of the ground electrode, the location of the DNA particles is brought closer to the ground electrode. The electric field is stronger around the particles, resulting in faster DNA motion. However, when all DNA particles are repelled, the lance direction parameter has a weak influence on the overall nanoinjection system (0% difference in the overall number of attracted and repelled DNA).

Ground Electrode Location

Consider the scenario where the ground electrode is the substrate (instead of a bond pad). For modeling purposes, we limit the substrate size to be 1111 μm by 1187 μm. Figure 4.9 shows the attracted results. Only 6 out of 50 particles were attracted to the lance while 5 out of the 6 attracted particles were repelled within the cell.

The results of the simulation when the ground electrode is placed under the lance show dramatic results. Only the nearest 6 DNA particles to the lance were attracted. The 44 others were

repelled by the substrate electrode and attracted to the input electrode. Because the input electrode is a material with a lower decomposition voltage than the lance material([32, 57]), more current will flow, moving more particles toward it. Figure 4.9 shows the attracted results. The majority of the trajectories are stopped when the DNA particles reached the bounds set by culture dish size and fluid volume. The ground electrode location parameter has a strong influence on the overall nanoinjection system (85% difference in the number of attracted DNA and 7.5% difference in the number of repelled DNA).

Lance Tip Width

The reference lance has a base width value of 11 μm and tapers to a 150 nanometer tip width. This value represents the minimal value constrained by the fabrication process. Because of this limitation, we increased the lance tip width in the comparison study. Increasing the tip width will increase the penetration contact surface area, likely increasing the damage cause upon injection. When the tip width is increased to 1 μm, most results remain unchanged with the exception of the number of repelled particles within the cell (37 compared to 36 for the reference simulation). The results show that the lance tip width has a weak influence factor on attraction and repulsion of DNA (0% difference in the number of attracted DNA and 2.5% difference in the number of repelled DNA). Hence it makes sense to minimize this parameter to keep cell trauma low.

Lance Tip Half Angle

The lance tip half angle is described as half the angle between the two sides of the lance. For a tip half angle value of 5°, the base width of the lance was changed from 11 μm to 21.9 μm. This allows the lance to be 124 μm long with a tip half angle value of 5° in comparison to 2.5° (the reference angle).

The number of attracted DNA particles increased slightly as the tip half angle increased (41 compared to 40). Because the base of the lance was doubled to keep the length at 124 μm, the first repulsed particles (closer to the base) travels a shorter distance negating the difference seen in time and distance. Overall, the tip half angle of the lance has a weak influence factor (2.5% difference

in the number of attracted DNA and 0.3% difference in the number of repelled DNA). Therefore it can be chosen to minimize injection force while retaining adequate stiffness, without regard to its effect on attraction and repulsion of DNA.

Lance Tip Height

The tip height parameter allows the lance to be transformed from a wedge of 1.5 micron thick into a pyramidal tip, shaping the lance more into a point rather than a wedge. This parameter can have the benefit of reducing cell trauma upon penetration of the lance but is significantly harder to fabricate than a wedge lance tip. For a 500 by 500 nanometers lance tip, the results in comparison to the reference simulations show little difference. Overall, the tip height of the lance has a weak influence factor (0% difference in the number of attracted and repelled DNA).

Lance Orientation

Another parameter of interest is the rotation of the lance 90 degrees such that it is oriented perpendicular to the substrate. The gap is increased to 200 μm to represent the vertical lance preparing to inject an egg cell below. The input electrode is placed directly above the lance (324 μm). 50 DNA particles are randomly placed between the ground and the input electrode. For the attractive model, 16 out of 50 particles were attracted to the rotated lance as shown in Figure 4.10. Results from rotating the lance 90 degrees clockwise are significant. Though the percentage of particles attracted to the lance is smaller than the reference simulation, it is still a significant fraction of the total particles. The lance orientation parameter has a strong influence when attracting DNA using nanoinjection (60% difference in the number of attracted DNA).

Even though the current design of the nanoinjector does not allow rotation of the lance, these simulation results show that research using a rotated lance prototype is feasible.

Penetration Depth

The depth of the lance inserted into the cell during injection is another important parameter. Consider 50% of the lance inserted into the cell in comparison to 75% of its length (the reference value). This study is only applicable during repulsion; therefore it will only be analyzed on the

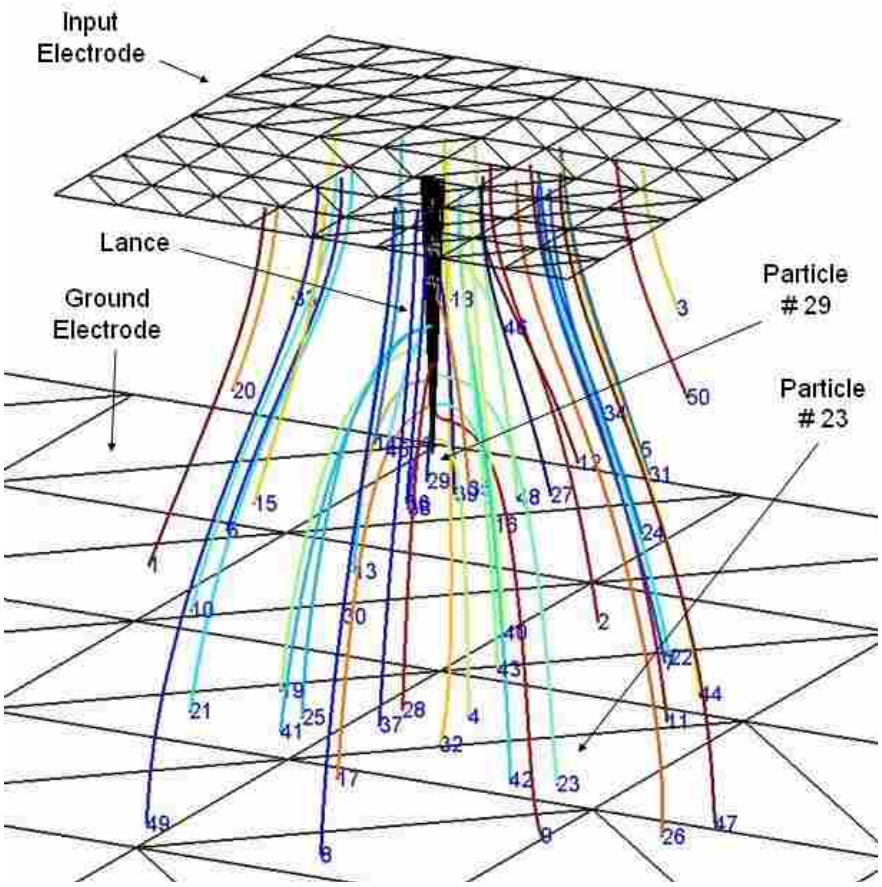

Figure 4.10: 16 out of 50 DNA particle attracted to the lance rotated 90° clockwise (lance orientation simulation)

repulsive model using the arrangement of attracted particles from the reference simulation. 32 out of 40 attracted particles were found within the cell. Figure 4.11 shows the repulsed results.

For the penetration depth parameter, only the repulsive model was relevant. Results show that the further into the cell the lance is projected, the DNA is repelled faster and the travelled distances are shorter. In addition, when the lance penetrates further into the cell, more of the DNA held on the lance enters the cell for repulsion. The penetration depth parameter has a strong influence when repelling DNA using nanoinjection (11% difference in the number of repelled DNA).

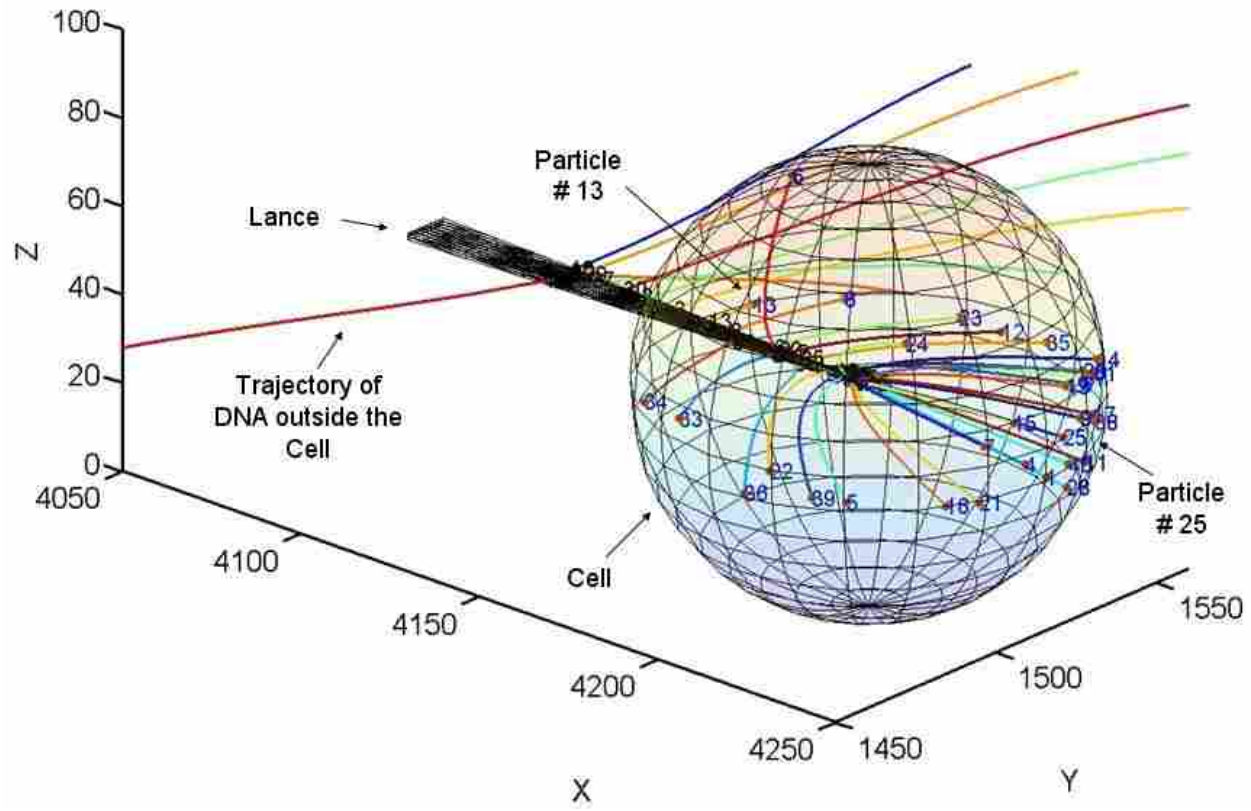

Figure 4.11: 40 DNA particle repelled from a lance penetrated half way through the cell (penetration depth simulation)

4.5 Conclusion

Both attractive and repulsive models were created with the intent to better understand the process of nanoinjection. By varying parameters within the models and comparing the results to a reference simulation, we are able to study and conclude which parameters have a stronger effect on attraction and repulsion of DNA during nanoinjection. The results from the reference simulation are the basis for the comparison study. The results are presented in Table 4.5. We classified each parameter as having either a weak influence or a strong influence affecting nanoinjection. Because nanoinjection is a co-joint process between attraction and repulsion, the influence of a parameter is ranked by its overall effect, not individually for attraction and repulsion independently. A weak influence is the result of a small compared difference on the overall nanoinjection. A strong influence for an individual parameter results in measurable differences affecting nanoinjection.

This comparison study determined that the gap (0% difference in the overall number of attracted and repelled DNA), lance direction (0% difference in the overall number of attracted and repelled DNA), lance tip width (0% difference in the number of attracted DNA and 2.5% difference in the number of repelled DNA), lance tip half angle (2.5% difference in the number of attracted DNA and .3% difference in the number of repelled DNA) and lance tip height (0% difference in the overall number of attracted and repelled DNA) were parameters that did not have a strong influence in affecting the nanoinjection process. This important results means that these parameters can be chosen for maximum mechanical efficiency, without regard to their effect on DNA motion. We furthermore conclude that the ground electrode placement, the lance orientation and the penetration depth are significant parameters that affect the nanoinjection process.

Ground electrode placement was shown to strongly affect the amount of DNA attracted to the lance (85% difference in the number of attracted DNA and 7.5% difference in the number of repelled DNA), with a ground electrode placed far from the lance performing better than one under the lance. We conclude that the ground electrode should be placed so that it is not directly under the lance. Further work should be performed to determined whether there is an optimal distance between the lance and the ground electrode.

Rotating the lance such that its orientation is perpendicular to the substrate was also shown to have a strong influence on DNA attraction (60% difference in the number of attracted DNA). Even though the input electrode is place directly above the lance, the percentage of particles attracted to the lance is still a significant fraction of the total particles. Perpendicular lances have the benefit of being able to inject many cells simultaneously. They can be fabricated as an array of lances used to deliver the same genetic material to a large number of cells at a time. This advantage may compensate for the smaller percentage of attracted particles.

The penetration depth was also a parameter that we classified as significant (11% difference in the number of repelled DNA). DNA is attracted to the lance in various locations as shown in Figure 4.7. The penetration depth exposes more surface area of the lance inside of the cell. This increases the total number of attracted particles to be repelled inside of the cell, allowing more of the DNA to reach the pronucleus. Hence, this study suggests that the lance should penetrate as far as possible into the cell to maximize the DNA particles injected into the cell.

CHAPTER 5. LOCALIZED ELECTROPORATION MODELING

5.1 Introduction

In addition to the study of parameters presented in chapter 4, we are interested in studying the electric field magnitude around the lance during injections(Figure 5.1). The results can be used to improve the nanoinjection design and process. The results also suggest that localized electroporation may significantly improve DNA transfer into the nucleus of a cell.

5.2 Cytoplasmic vs Pronuclear Injection

Current technology relies on injection into an egg cell's pronucleus to obtain integration of new substances for genetic modifications. Duplication of the genetic material only takes place inside of the pronucleus. This method requires a trained technician to operate the process, providing limited and slow results. Cytoplasmic injection, on the other hand, is a non targeted injection anywhere inside the injected cell. This method has the benefit of allowing automation, resulting in a continuous, large output quantity. However, this method requires the injected substance to travel to the pronucleus for any hope of integration, resulting in an unreliable process [1]. Methods such as electroporation can help the cytoplasmic process by increasing the permeability of the cell membranes. In electroporation, an electric field causes pores to open in cell membranes, allowing macromolecules such as DNA to pass through the membranes, including the nuclear membranes. Literature suggests that electroporation occurs for field strength between 100 to 200 V/cm [70].

We propose that cytoplasmic injection using nanoinjection can cause localized electroporation and DNA motion sufficient to reach the pronucleus. We will test this hypothesis by modeling the electric field magnitude in a cell during nanoinjections.

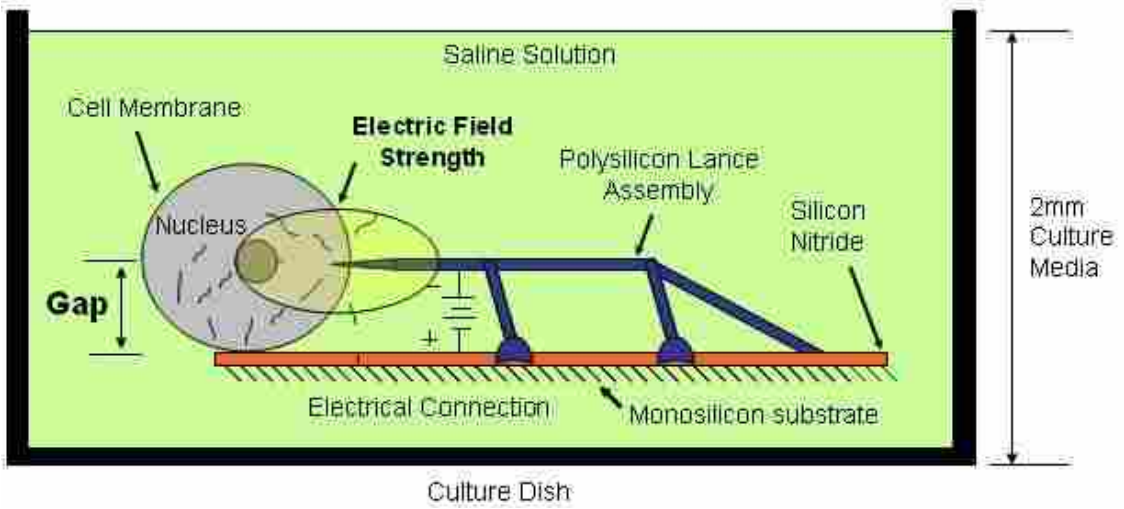

Figure 5.1: Representation of the electric field around the lance overlapping a cell

5.3 Study of Electric Field Strength

Sufficient electric field strength can cause electroporation (increased permeability of cell membranes, including nuclear membranes). Electroporation is usually used in molecular biology as a way of introducing substances into a cell. We hypothesize that nanoinjection may create a zone of localized electroporation for transfer of DNA into the nucleus of a cell. To study this effect, we use the model to predict the size of a zone around the lance which has electric field magnitude above a threshold value. We then compare the resulting zone with the expected location of the pronucleus in a fertilized egg.

5.3.1 Calculating the Electric Field Envelope

The charges collected on the surface of the lance create an electric field. The electric field may cause electroporation which increases the permeability of the cell membrane. Prior literature suggests that electroporation occurs at a field strength of 100-200 V/cm [70]. It is of interest to investigate the physical size of a 200 V/cm electric field around the lance versus the diameter of the cell and the time duration for all particles to reach the outer edge of the field.

As stated by equation 2.4, an electric field is said to exist in the region of space around charged objects. The magnitude of the electric field at any point inside the region of space is strongly dependant on the location of that point. Therefore, there exist a location of points for

which the electric field is the same. This location of points is referred to as the electric field envelope.

Given the charges located on the lance, input electrode, and ground electrode, the magnitude of the electric field is numerically calculated using the mathematical model. An automated routine is added to the mathematical model to randomly select points around the lance. The routine evaluates the electric field at each point, and saves the locations of points with an electric field magnitude with a certain tolerance of the desired magnitude. The routine then randomly selects additional points, and again evaluates them to determine those with the desired field strength. The routine stops when the desired number of points specified by the user is obtained. An additional routine to create surfaces from points is used to map the volumetric shape of the envelope.

5.3.2 Results

Figure 5.2 shows the cell, the lance, the electric field of value 200 V/cm and the DNA repulsed to the outer edge of the field. The first repulsed particle displaced 9.58 μm in 1.2 ms (particle number 4). The last repulsed particle displaced 19.59 μm in 2.6 ms (particle number 13).

The electric field strength was studied to visually see how far around the lance the volume of a field magnitude envelope reached. Even though the electric field envelope of value 200 V per cm around the lance is 2.5 times smaller than the cell, we expect the DNA to be repelled 2.5 times faster. In fact, it is almost 5 times faster. This nonlinearity is explained from the field strength being inversely proportional to the square of the distance.

A recent study by our group [71] was conducted to measure the distance between the center of the female pronucleus (15 μm diameter) and the center of the cell (100 μm diameter) over time. Nanoinjection occurs between 21 hrs (time A) and 28 hrs (time B) post hCG (human chorionic gonadotropin) injection into the mouse egg donor. Figures 5.3(a), 5.3(b), 5.3(c) show the average location of the center of the pronucleus (anywhere on that circle) at time A and time B. The data is based on 105 measurements made on 29 cells as a function of time with a standard deviation of 4.5 micron. Over time, the pronucleus moves toward the center of the cell. Note that between time A and time B (the time interval for performance of nanoinjection experiments), the center of the pronucleus is always within within the 200 V/cm volume. This supports our hypothesis that

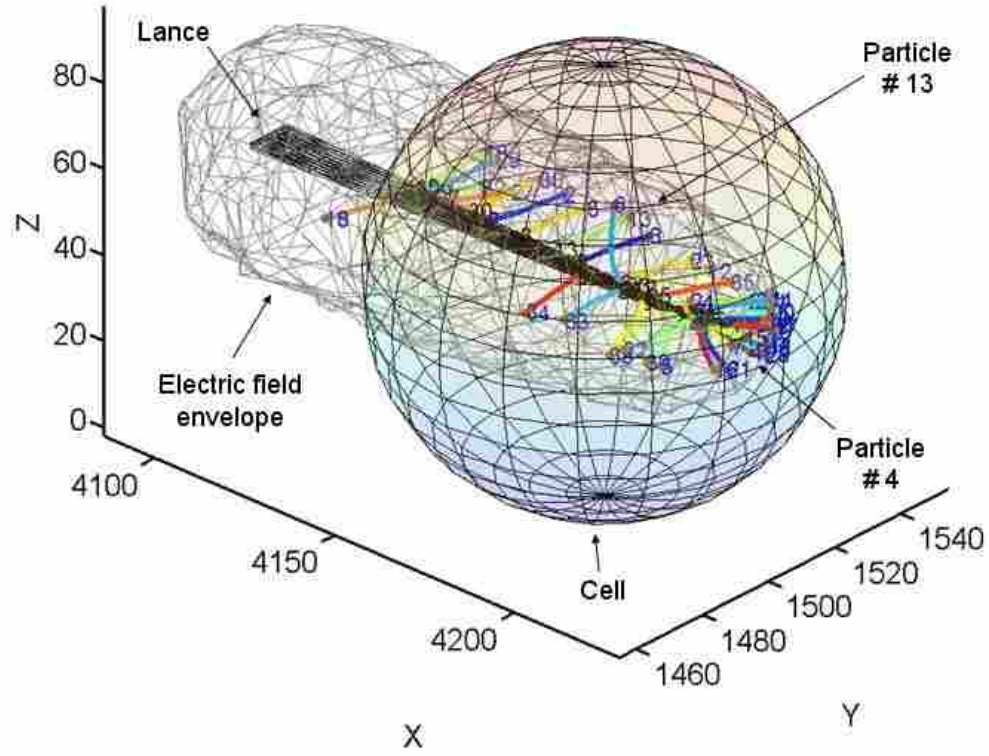

Figure 5.2: Electric field envelope at 200 V per cm

nanoinjection will create a zone of localized electroporation for transfer of DNA into the nucleus of a cell.

5.4 Conclusion

We created a model that physically shows the electric field envelope of value 200 V/cm around the lance and calculates the time necessary for all particles to reach the outer edge of the field. An electric field of this magnitude causes electroporation which increases the permeability of the cell membrane. The location of the pronucleus of the cell was found to lie within the electric field envelope, increasing the likelihood of DNA being repelled into the pronucleus. Electroporation can be used as a way of introducing substances into a cell, increasing the efficiency of the nanoinjector.

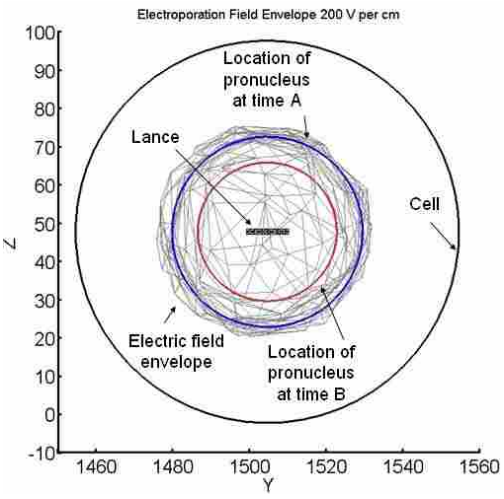

(a) front view

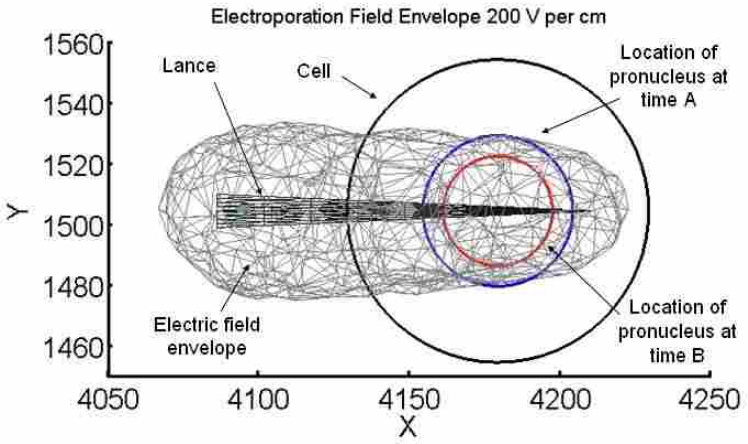

(b) Top view

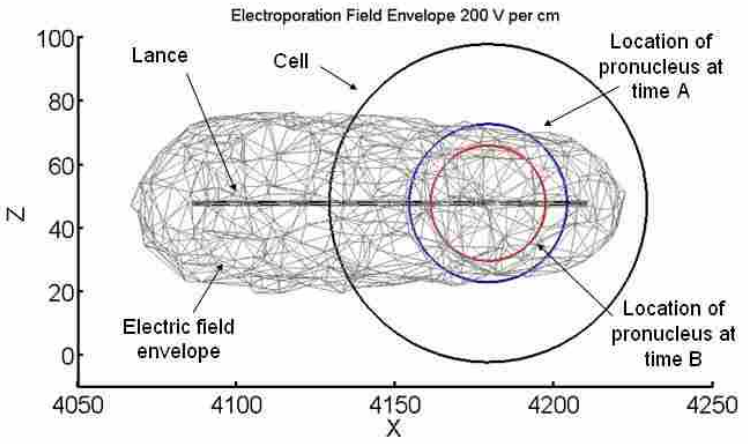

(c) Side view

Figure 5.3: Electric field results

CHAPTER 6. CONCLUSION

The work in this dissertation describes a mathematical model proposed to simulate the motion of DNA using nanoinjection. The model predicts the electric behavior around the lance due to the potential difference between the lance/input electrode and the ground electrode. No exact closed-form solution is available for the complex geometry; therefore, a numerical solution was developed. The Boundary Element Method (BEM) is used to calculate the charge density on each electrode. The resulting charge distribution collected on the surfaces of the electrodes is then used to calculate the electric field. The model predicts the macromolecular motion of DNA due to the electric field created from the charges on the surfaces of the conductors. An applied electric force, a viscous resistive force, and an electrophoretic retardation force are considered to act on a DNA particle. The sum of the forces defines the acceleration of the particle. The position and velocity can then be determined from the acceleration.

This work also described the protocol for DNA motion using fabricated macroscale gel electrophoresis devices. Experiments to monitor and understand the displacement of DNA as a function of voltage, ionic concentration and DNA base pair size were conducted. The DNA was stained using EtBr, and microscope images (using UV light) were recorded at separate time intervals. MATLAB was used as the post processor to analyze pixel motion within each image saved. The results for each set of experiments were presented as a velocity vs. voltage plot. From the results, we can conclude that the velocity of DNA is correlated directly to current flow, which in turn is controlled by the ionic solution and the voltage applied to the device.

The experimental voltage vs velocity curve was used to verify the mathematical model for predicting the motion of DNA. The simulated model provides results similar to the experimental results. The good agreement between the model and the experiments validates the model's predictions. The model is verified and validated, including the prediction of accurate curved motion of

DNA in the presence of a non-uniform electric field with an accuracy within 4% of experimental results.

This work also studied the effects of different electrode material on decomposition voltage, electrical field and DNA motion. Experimental results were used to update the mathematical model to reflect the differences in material. We also showed that our model predicts large curved-field motion of charged particles during electrophoresis. To see how adaptable the mathematical model is to different electrode configurations, two thin steel electrodes were placed at an offset diagonal of each other. The results showed that the motion of DNA is multi-directional and follows the electric field.

A more representative electrode set up for the nanoinjector was studied (three electrodes representing two electrical connections and the tip of the lance). We conducted an experiment using 3 steel electrodes. The model can be used to accurately predict motion of DNA under 2 or 3 steel electrodes (independent of spatial positioning). Because the nanoinjection lance is fabricated from silicon, we studied material effect on DNA motion. To test the hypothesis that electrode material (Si and St) does affect the motion of particles, we conducted a set of experiments at 10 V and at 5 V. The results show that electrode material does have a significant effect on DNA motion, especially when the applied voltage is near the decomposition voltage for the system. We also showed excellent correlation between experimental results and simulations, indicating the power of the model in predicting DNA motion. The next step is to use the model to study and improve the nanoinjection process.

Both attractive and repulsive models were created with the intent to better understand the process of nanoinjection. By varying parameters within the models and comparing the results to a reference simulation, we are able to study and conclude which parameters have a stronger effect on attraction and repulsion of DNA during nanoinjection. The results from the reference simulation are the basis for the comparison study. The results are presented in Table 4.5. We classified each parameter as having either a weak influence or a strong influence affecting nanoinjection. Because nanoinjection is a co-joint process between attraction and repulsion, the influence of a parameter is ranked by the overall number of DNA molecules attracted and repelled during nanoinjection. A weak influence is the result of a small compared difference of the number of attracted and repelled

DNA molecules between the reference and the comparison simulations (less than 5% difference). A strong influence for an individual parameter results from a compared difference greater than 5%.

This comparison study determined that the gap (0% difference in the overall number of attracted and repelled DNA), lance direction (0% difference in the overall number of attracted and repelled DNA), lance tip width (0% difference in the number of attracted DNA and 2.5% difference in the number of repelled DNA), lance tip half angle (2.5% difference in the number of attracted DNA and 0.3% difference in the number of repelled DNA) and lance tip height (0% difference in the overall number of attracted and repelled DNA) were parameters that did not have a strong influence in affecting the nanoinjection process. This important results means that these parameters can be chosen for maximum mechanical efficiency, without regard to their effect on DNA motion. We furthermore concluded that the ground electrode placement, the lance orientation and the penetration depth are significant parameters that affect the nanoinjection process.

Ground electrode placement was shown to strongly affect the amount of DNA attracted to the lance (85% difference in the number of attracted DNA and 7.5% difference in the number of repelled DNA), with a ground electrode placed far from the lance performing better than one under the lance. We concluded that the ground electrode should be placed so that it is not directly under the lance. Further work should be performed to determined whether there is an optimal distance between the lance and the ground electrode.

Rotating the lance such that its orientation is perpendicular to the substrate was also shown to have a strong influence on DNA attraction (60% difference in the number of attracted DNA). Even though the input electrode is place directly above the lance, the percentage of particles attracted to the lance is still a significant fraction of the total particles. Perpendicular lances have the benefit of being able to inject many cells simultaneously. They can be fabricated as an array of lances used to deliver the same genetic material to a large number of cells at a time. This advantage may compensate for the smaller percentage of attracted particles.

The penetration depth was also a parameter that was classified as significant (11% difference in the number of repelled DNA). DNA is attracted to the lance in various locations as shown in Figure 4.7. The penetration depth exposes more surface area of the lance inside of the cell. This increases the total number of attracted particles to be repelled inside of the cell, allowing more of

the DNA to reach the pronucleus. Hence, this study suggests that the lance should penetrate as far as possible into the cell to maximize the DNA particles injected into the cell.

In addition, a physical representation of an electric field envelope was added to the model. For a value of 200 V/cm around the lance, the time necessary for all particles to reach the outer edge of the field was calculated. An electric field of this magnitude causes electroporation, which increases the permeability of the cell membrane. The location of the pronucleus of the cell was found to lie within the electric field envelope, increasing the likelihood of DNA being repelled into the pronucleus. Electroporation can thus be used as a way of introducing substances into a cell, increasing the efficiency of the nanoinjector, and providing evidence that nanoinjection into a cell's cytoplasm may be used to transport DNA into the pronucleus.

6.1 Summary of Contributions

The primary contributions of this work are as follows:

- I developed an analytical model capable of predicting the electric field around complex geometry (vicinity of the lance) and modeled the macromolecular motion (attraction and repulsion) due to the electric field in a saline solution.
- I tested and validated the model against experimental DNA motion as a function of time, under electrostatic forces, in saline solution between stainless steel parallel plates.
- I extended experimental testing and validation of the model to predict large curved field motion of charged particles during electrophoresis and studied the effects of dissimilar electrode material (steel and silicon) on decomposition voltage, electrical field and DNA motion.
- I performed a comparison study of design parameters (using the model) to identify ways to improve the efficiency of nanoinjection.
- I included a study of the electric field strength sufficient to cause localized electroporation to facilitate DNA transfer to the pronucleus.
- I have published two conference papers on this work.

- I have published one journal paper and prepared two additional journal papers for submission. A fourth paper describing localized electroporation is planned.

6.2 Suggested Future Work

Additional research is needed to further develop the nanoinjector system. Some suggestions are proposed but not limited to:

1. Design and test a lance perpendicular to its substrate
2. Complete experiments to validate the electroporation hypothesis
3. Fabricate and test different ground electrode locations
4. Fabricate a force gauge mechanism to study the range of forces required to puncture the cell membranes
5. Design, fabricate and model a 'stand alone' lance (currently under study)
6. Implement findings from Chapter 4 to current design of nanoinjection

6.3 Closing Statements

This research has led to the development of a mathematical model to accurately describe and predict motion of DNA using electrical forces inside a saline solution using different electrode material. Some potential applications which will benefit from this new tool are primarily new ways to deliver genetic material, including medication, to advance genetic research and engineering at a fraction of the current cost. The significance of this research is not limited to academic publications. This method could have a significant impact on health care, elimination of specific diseases, increase quality and longevity of life, provide an additional solution to infertility and advance research in cloning. This work is significant because it provides a solution to a new method to deliver genetic material no one considered or knew would work. This led to the challenge of an in depth study to predict the behavior of DNA motion and its effect on design parameters for optimized designs of this new method. Also, with an accurate simulation, it may reduce the amount of laboratory work required to develop and optimized this new technique. More of the development

may be tested by simulation, allowing improvements in geometry, materials, and techniques before actual test are performed.

REFERENCES

[1] Brinster, R. L., Chen, H. Y., Trumbauer, M. E., Yagle, M. K., and Palmiter, R. D., 1985. "Factors affecting the efficiency of introducing foreign DNA into mice by microinjecting eggs." *Proceedings of the National Academy of Sciences,* **82**(13), July, pp. 4438–4442.

[2] Gordon, J. W., Scangos, G. A., Plotkin, D. J., Barbosa, J. A., and Ruddle, F. H., 1980. "Genetic transformation of mouse embryos by microinjection of purified DNA." *Proceedings of the National Academy of Sciences,* **77**(12), December, pp. 7380–7384.

[3] Aten, Q. T., 2008. "Design and testing of a pumpless microelectromechanical system nanoinjector." Master's thesis, Brigham Young University.

[4] Yamauchi, Y., Doe, B., Ajduk, A., and Ward, M., 2007. "Genomic DNA damage in mouse transgenesis." *Biology of Reproduction,* **77**(3), November, pp. 803–812.

[5] Wall, R. J., 2001. "Pronuclear microinjection." *Cloning and Stem Cells,* **3**(4), December, pp. 209–220.

[6] Zappe, S., Fish, M., Scott, M., and Solgaard, O., 2006. "Automated MEMS-based drosophila embryo injection system for high-throughput RNAi screens." *Lab on a Chip,* **6**, pp. 1012–1019.

[7] Wong, P., Ulmanella, U., and Ho, C., 2004. "Fabrication process of microsurgical tools for single-cell trapping and intracytoplasmic injection." *Microelectromechanical Systems, Journal of,* **13**(6), December, pp. 940–946.

[8] Carter, J., Cowen, A., Hardy, B., Mahadevan, R., Stonefield, M., and Wilcenski, S., 2005. *PolyMUMPs Design Handbook Revision 11*. MEMSCAP Inc.

[9] Subirana, J., and Soler-Lopez, M., 2003. "Cations as hydrogen bond donors: A view of electrostatic interactions in DNA." *Annual Review of Biophysics and Biomolecular Structure,* **32**(1), pp. 27–45.

[10] Liu, C., 2006. *Foundations of MEMS*. Pearson, Prentice Hall.

[11] Pethig, R., 1984. "Dielectric properties of biological materials: Biophysical and medical applications." *Electrical Insulation, IEEE Transactions on,* **EI-19**(5), October, pp. 453–474.

[12] Pohl, H. A., 1978. *Dielectrophoresis: the behavior of neutral matter in nonuniform electric fields*. Cambridge University Press.

[13] Mohanty, S. K., Rawla, S. K., Engisch, K. L., and Frazierl, A. B., 2003. "A micro system using dielectrophoresis and electrical impedance spectroscopy for cell manipulation and analysis." *The 12th International Conference on Solid State Sensors, Actuators and Microsystems*, June, pp. 1055–1058.

[14] Asbury, C. L., Diercks, A. H., and van den Engh, G., 2002. "Trapping of DNA by dielectrophoresis." *Electrophoresis,* **23**(16), Aug, pp. 2658 – 2666.

[15] Woolley, A. T., Hadley, D., Landre, P., deMello, A. J., Mathies, R. A., and Northrup, M. A., 1996. "Functional integration of PCR amplification and capillary electrophoresis in a microfabricated DNA analysis device." *Analytical Chemistry,* **68**, pp. 4083–4086.

[16] Washizu, M., Suzuki, S., Kurosawa, O., Nishizaka, T., and Shinohara, T., 1994. "Molecular dielectrophoresis of biopolymers." *IEEE Transactions on Industry Applications,* **30**(4), July / August, pp. 835–843.

[17] Hughes, M. P., 2002. "Dielectrophoretic behavior of latex nanospheres: Low-frequency dispersion." *Journal of Colloid and Interface Science,* **250**.

[18] Zheng, L., Brody, J. P., and Burke, P. J., 2004. "Electronic manipulation of DNA, proteins, and nanoparticles for potential circuit assembly." *Biosensors and Bioelectronics,* **20**, pp. 606–619.

[19] Helling, R., Goodman, H., and Boyer, H., 1974. "Analysis of endonuclease REco RI fragments of DNA from lambdoid bacteriophages and other viruses by agarose-gel electrophoresis." *Journal of Virology,* **14**(5), November, pp. 1235–1244.

[20] Maniatis, T., Jeffrey, A., and Van deSande, H., 1975. "Chain length determination of small double-and single-stranded DNA molecules by polyacrylamide gel electrophoresis." *Biochemistry,* **14**(17), pp. 3787–3794.

[21] Mastrangelo, C., Burns, M., and Burke, D., 1998. "Microfabricated devices for genetic diagnostics." *Proceedings of the IEEE,* **86**(8), August, pp. 1769–1787.

[22] Burns, M., Johnson, B., Brahmasandra, S., Handique, K., Webster, J., Krishnan, M., Sammarco, T., Man, P., Jones, D., Heldsinger, D., Mastrangelo, C., and Burke, D., 1998. "An integrated nanoliter DNA analysis device." *Science,* **282**, October, pp. 484–487.

[23] Pei, H., Allison, S., Haynes, B. M., and Augustin, D., 2009. "Brownian dynamics simulation of the diffusion of rods and wormlike chains in a gel modeled as a cubic lattice: Application to DNA." *The Journal of Physical Chemistry B,* **113**(9), pp. 2564–2571.

[24] Sun, Y., Kwok, Y. C., and Nguyen, N.-T., 2007. "Modeling and experimental characterization of peak tailing in DNA gel electrophoresis." *Microfluidics and Nanofluidics,* **3**(3), June, pp. 323–332.

[25] Radivoyevitch, T., and Cedervall, B., 1996. "Mathematical analysis of DNA fragment distribution models used with pulsed-field gel electrophoresis for DNA double-strand break calculations." *Electrophoresis,* **17**(6), pp. 1087–1093.

[26] Barkema, G. T., Caron, C., and Marko, J. F., 1996. "Scaling properties of gel electrophoresis of DNA." *Biopolymers,* **38**, pp. 665–667.

[27] Pernodet, N., and Tinland, B., 1997. "Influence of λ-DNA concentration on mobilities and dispersion coefficients during agarose gel electrophoresis." *Biopolymers,* **42**(4), pp. 471–478.

[28] Lee, N., Obukhov, S., and Rubinstein, M., 1996. "Deterministic model of DNA gel electrophoresis in strong electric fields." *Electrophoresis,* **17**(6), pp. 1011–1017.

[29] Allison, S. A., Pei, H., and Xin, Y., 2007. "Modeling the free solution and gel electrophoresis of biopolymers: The bead array-effective medium model." *Biopolymers,* **87**(2-3), July, pp. 102–114.

[30] Krawczyk, M., Pasciak, P., Dydejczyk, A., and Kulakowski, K., 2005. "Gel electrophoresis of DNA new measurements and the repton model at high fields." *Acta Physica Polonica B,* **36**(5), pp. 1653–1662.

[31] Newman, M. E. J., and Barkema, G. T., 1997. "Diffusion constant for the repton model of gel electrophoresis." *Physical Review E,* **56**(3), September, pp. 3468–3473.

[32] David, R. A., Jensen, B. D., Black, J. L., Burnett, S. H., and Howell, L. L., 2010. "Modeling and experimental validation of DNA motion in uniform and non-uniform DC electric fields." *Journal of Nanotechnology in Engineering and Medicine, NANO-10-1049*.

[33] Aten, Q. T., Jensen, B. D., and Burnett, S. H., 2008. "Testing of a pumpless MEMS microinjection needle employing electrostatic attraction and repulsion of DNA." In *2008 Proceedings of the ASME Micro-Nano Systems Conference, DETC2008-49548*.

[34] Viovy, J.-L., 2000. "Electrophoresis of DNA and other polyelectrolytes: Physical mechanisms." *Reviews of Modern Physics,* **72**(Issue 3), pp. 813–872.

[35] Slater, G. W., Desruisseaux, C., and Hubert, S. J., 2001. "DNA separation mechanisms during electrophoresis." In *Capillary Electrophoresis of Nucleic Acids Volume 1: Introduction to the Capillary Electrophoresis of Nucleic Acids*, K. R. Mitchelson and J. Cheng, eds., Vol. 162 of *Methods In Molecular Biology*. Humana Press, pp. 27–41.

[36] Allen, R. C., and Budowle, B., 1994. *Gel Electrophoresis of Proteins and Nucleic Acids*. Walter de Gruyter & Co.

[37] Audubert, R., and de Mende, S., 1960. *The Principles of Electrophoresis*. The Macmillan Company.

[38] Martin, R., 1996. *Gel Electrophoresis: Nucleic Acids*. BIOS Scientific Publishers Limited.

[39] Brebbia, C. A., Telles, J. C. F., and Wrobel, L. C., 1984. *Boundary Element Techinques: Theory and Applications in Engineering*. Springer-Verlag.

[40] Mei, W. N., and Holloway, A., 2005. "Electrostatics of a point charge between intersecting planes: exact solutions and method of images." *International Journal of Mathematical Education in Science and Technology,* **36**(8), pp. 843–860.

[41] Coco, S., and Ragusa, C., 2000. "Accurate computation of local and global electrostatic quantities from FE solution." *IEEE Transactions on Magnetics,* **36**(4), JULY.

[42] Cady, W. G., 1935. "The potential distribution between parallel plates and concentric cylinders due to any arbitrary distribution of space charge." *Physics,* **6**.

[43] Klein, L. A., and Swift, C. T., 1977. "An improved model for the dielectric constant of sea water at microwave frequencies." *lEEE Transactions on Antennas and Propagation,* **AP-25**(1), January, pp. 104–111.

[44] Stogryn, A., Aug 1971. "Equations for calculating the dielectric constant of saline water." *Microwave Theory and Techniques,* **19, Issue: 8**, pp. 733– 736.

[45] Ellison, W., Balana, A., Delbos, G., Lamkaouchi, K., Eymard, L., Guillou, C., and Prigent, C., 1998. "New permittivity measurments of seawater." *Radio Science,* **33**(3), May-June, pp. 639–648.

[46] Blanch, S., and Aquasca, A., 2004. "Seawater dielectric permittivity model from measurements at L band." *Geoscience and Remote Sensing Symposium,* **2**, September, pp. 1362–1365.

[47] Meissner, T., and Wentz, F. J., 2004. "The complex dielectric constant of pure and sea water from microwave satellite observations." *Geoscience and Remote Sensing,* **42**(9), September, pp. 1836–1849.

[48] Somaraju, R., and Trumpf, J., 2006. "Frequency, temperature and salinity variation of the permittivity of seawater." *Antennas and Propagation,* **54**(11), November, pp. 3441–3448.

[49] Hickey, J. D., Hellerb, L., Hellerc, R., and Gilberta, R., 2005. "Electric field mediated DNA motion model." *Bioelectrochemistry,* **70**(1), June, pp. 101–103.

[50] Morrison, I. D., and Ross, S., 2002. *Colloidal dispersions, suspensions, emulsions and foams*. Wiley-Interscience.

[51] Everett, D. H., 1988. *Basic principles of colloid science*. Royal Society of Chemestry.

[52] Bier, M., ed., 1967. *Electrophoresis Theory, Methods, and Applications*., Vol. II Academic Press Inc.

[53] Bier, M., ed., 1959. *Electrophoresis Theory, Methods, and Applications*., Vol. I Academic Press Inc.

[54] Shaw, D. J., 1969. *Electrophoresis*. Academic Press Inc.

[55] Mosher, R. A., Saville, D. A., and Thormann, W., 1992. *The Dynamics of Electrophoresis*. VCH Publishers Inc.

[56] David, R. A., and Jensen, B. D., 2009. "Modeling DNA motion under electrostatic repulsion within a living cell." In *2009 Proceedings of the ASME Micro-Nano Systems Conference, DETC2009-87413*.

[57] David, R. A., Black, J. L., Jensen, B. D., and Burnett, S. H., 2010. "Modeling and experimental validation of DNA motion during electrophoresis." In *2010 Proceedings of the ASME Micro-Nano Systems Conference, DETC2010-28541*.

[58] Li, B., Fang, X., Luo, H., Petersen, E., Seo, Y.-S., Samuilov, V., Rafailovich, M., Sokolov, J., Gersappe, D., and Chu, B., 2006. "Influence of electric field intensity, ionic strength, and migration distance on the mobility and diffusion in DNA surface electrophoresis." *Electrophoresis,* **27**, p. 13121321.

[59] Slater, G. W., Guillouzic, S., Gauthier, M. G., Mercier, J.-F., Kenward, M., McCormick, L. C., and Tessier, F., 2002. "Theory of DNA electrophoresis." *Electrophoresis,* **23**, p. 37913816.

[60] Rickwood, D., and Hames, B. D., eds., 1990. *Gel Electrophoresis of Nucleic Acids*., second ed. Oxford University Press.

[61] Chrambach, A., 1985. *The Practice of Quantitative Gel Electrophoresis*., first ed. Deutsche Bibliothek Cataloguing-in-Publication-Data.

[62] Wieme, R. J., 1965. *Agar Gel Electrophoresis*. Elsevier Publishing Company.

[63] Schuler, T., Kretschmer, R., Jessing, S., Urban, M., Fritzsche, W., Moller, R., and Popp, J., 2009. "A disposable and cost efficient microfluidic device for the rapid chip-based electrical detection of DNA." *Biosensors and Bioelectronics,* **25**, May, pp. 15–21.

[64] Rogers, W. E., 1954. *Introduction to electric fields*. McGraw Hill.

[65] Morse, P. M., and Feshback, H., 1953. *Methods of Theoretical Physics*., Vol. I McGraw Hill.

[66] Morse, P. M., and Feshback, H., 1953. *Methods of Theoretical Physics*., Vol. II McGraw Hill.

[67] Zhu, M. W., Li, H. W., Chen, X. L., Tang, Y. F., Lu, M. H., and Chen, Y. F., 2009. "Silica needle template fabrication of metal hollow microneedle arrays." *Journal of Micromechanics and Microengineering,* **19**(11), October.

[68] Chaudhri, B. P., Ceyssens, F., Moor, P. D., Hoof, C. V., and Puers, R., 2010. "A high aspect ratio su-8 fabrication technique for hollow microneedles for transdermal drug delivery and blood extraction." *Journal of Micromechanics and Microengineering,* **20**(6), June.

[69] Khanna, P., Luongo, K., Strom, J. A., and Bhansali, S., 2010. "Sharpening of hollow silicon microneedles to reduce skin penetration force." *Journal of Micromechanics and Microengineering,* **20**(4), March.

[70] Grabarek, J. B., Plusa, B., Glover, D. M., and Zernicka-Goetz, M., 2002. "Efficient delivery of dsRNA into zona-enclosed mouse oocytes and preimplantation embryos by electroporation." *Genesis,* **32**(4), April, pp. 269–276.

[71] L.Black, J., and Burnett, S. H., 2010. Pronuclear migration in the mouse zygote indicates a bi-phasic movement of the female pronucleus.